Inducible and reversible phenotypes in a novel mouse model of Friedreich's Ataxia

Vijayendran Chandran[1,#], Kun Gao[1], Vivek Swarup[1], Revital Versano[1], Hongmei Dong[1], Maria C. Jordan[3] & Daniel H. Geschwind[1,2]

[1]Program in Neurogenetics, Department of Neurology, [2]Department of Human Genetics, [3]Department of Physiology, David Geffen School of Medicine, University of California, Los Angeles, CA 90095, USA.
[#]Present address: Department of Pediatrics, School of Medicine, University of Florida, Gainesville, FL 32610-0296, USA.
Correspondence should be addressed to D.G. (dhg@mednet.ucla.edu) or V.C. (vijayendran@ufl.edu).

Abstract

Friedreich's ataxia (FRDA), the most common inherited ataxia in humans, is caused by recessive mutations that lead to a substantial reduction in the levels of frataxin (FXN), a mitochondrial iron binding protein. FRDA is a multi-system disease, involving multiple neurological, cardiac, and metabolic manifestations whose study would be substantially advanced by animal models that faithfully recapitulate human disease features. We developed an inducible mouse model of *Fxn* deficiency that enabled us to control the onset, progression and potential rescue of disease phenotypes by the modulation of *Fxn* levels using RNA interference. We found that systemic knockdown of *Fxn* in adult mice led to multiple features paralleling those observed in human patients, including electrophysiological, cellular, biochemical and structural phenotypes associated with cardiomyopathy, as well as dorsal root ganglion and retinal neuronal degeneration and reduced axonal size and myelin sheath thickness in the spinal cord. *Fxn* knockdown mice also exhibited other abnormalities similar to patients, including weight loss, reduced locomotor activity, ataxia, reduced muscular strength, and reduced survival, as well as genome-wide transcriptome changes. The reversibility of knockdown also allowed us to determine to what extent observed phenotypes represent neurodegenerative cell death, or reversible cellular dysfunction. Remarkably, upon restoration of near wild-type FXN levels, we observed significant recovery of function, pathology and associated transcriptomic changes, even after significant motor dysfunction was observed. This inducible model of FRDA is likely to be of broad utility in therapeutic development and in understanding the relative contribution of reversible cellular dysfunction to the devastating phenotypes observed in this condition.

Introduction

A guanine-adenine-adenine (GAA) trinucleotide repeat expansion within the first intron of the frataxin (*Fxn*) gene in the chromosome 9 is the major cause of Friedreich's ataxia (FRDA), the most commonly inherited ataxia[1,2]. Due to recessive inheritance of this GAA repeat expansion, patients have a marked deficiency of *Fxn* mRNA and protein levels caused by reduced *Fxn* gene transcription[2,3]. Indeed, the GAA expansion size has been shown to correlate with residual *Fxn* levels, earlier onset and increased severity of disease[4,5]. The prevalence of heterozygous carriers of the GAA expansion is between 1:60 and 1:110 in European populations, and the heterozygous carriers of a *Fxn* mutation are not clinically affected[6,7].

FRDA is an early-onset neurodegenerative disease that progressively impairs motor function, leading to ataxic gait, cardiac abnormalities, and other medical co-morbidities, ultimately resulting in early mortality (median age of death, 35 years)[8,9]. However, identification of the causal gene led to identification of a significant number of patients with late onset, they tend to have slower progression with less severe phenotype and are associated with smaller GAA expansions[10]. This shorter expansion enables residual *Fxn* expression[11], thus modifying the classical FDRA phenotype, consistent with other data indicating that *Fxn* deficiency is directly related to the FRDA phenotype[12]. Extra-neurologic symptoms including metabolic dysfunction and insulin intolerance are observed in the majority and frank type I diabetes is observed in approximately 15% of patients, the severity of which is related to increasing repeat length[13-15]. The mechanisms by which *Fxn* reduction leads to clinical symptoms and signs remain to be elucidated, but molecular and cellular dysfunction mediated by a critical reduction in *Fxn* levels plays a central role[16].

FXN is a nuclear-encoded mitochondrial protein involved in the biogenesis of iron-sulphur clusters, which are important for the function of the mitochondrial respiratory chain activity[17,18]. Studies in mouse have shown that *Fxn* plays an important role during embryonic development, as homozygous frataxin knockout mice display embryonic lethality[19], consistent with FXN's evolutionary conservation from yeast to human[2,3]. Over the past several years, multiple mouse models of frataxin deficiency, including a knock-in knockout model[20], repeat expansion knock-in model[20], transgenic mice containing

the entire *Fxn* gene within a human yeast artificial chromosome, YG8R and YG22R[21,22], as well as a conditional *Fxn* knockout mouse, including the cardiac-specific[23] and a neuron specific model[23] have been generated. These existing transgenic and heterozygous knockout FRDA animal models are either mildly symptomatic, or restricted in their ability to recapitulate the spatial and temporal aspects of systemic FRDA pathology when they are engineered as tissue-specific conditional knockouts[20-25]. Despite advances made towards elucidating FRDA pathogenesis, many questions remain due to the need for mouse models better recapitulating key disease features to understand frataxin protein function, disease pathogenesis and to test therapeutic agents.

In this regard, one crucial question facing therapeutic development and clinical trials in FRDA is the reversibility of symptoms. The natural history of the disorder has been well described[26,27], it is not known how clinical features such as significant motor disability relate to reversible processes (e.g. underlying neuronal dysfunction) or reflect irreversible cell death. It is often assumed that clinically significant ataxia and motor dysfunction reflects neurodegeneration, although this may not be the case. This issue, while critically important for therapeutic development, is difficult to address in patients, but we reasoned that we could begin to address this question in an appropriate mouse model.

Here we report an inducible mouse model for FRDA, the FRDAkd mouse, that permits reversible, and yet substantial frataxin knockdown, allowing detailed studies of the temporal progression, or recovery following restoration of frataxin expression - the latter permitting exploration of disease reversal given optimal treatment (normalization of *Fxn* levels). We observe that *Fxn* knockdown leads to behavioral, physiological, pathological and molecular deficits in FRDAkd mice paralleling those observed in patients, including severe ataxia, cardiac conduction defects and increased left ventricular wall thickness, iron deposition, mitochondrial abnormalities, low aconitase activity, and degeneration of dorsal root ganglia, retina, as well as early mortality. We identify a signature of molecular pathway dysfunction via genome-wide transcriptome analyses, and show reversal of this molecular phenotype and as well as behavioral and pathological measures, even in the setting of significant disability due to motor dysfunction in FRDAkd animals.

RESULTS

RNA interference based in vivo frataxin knockdown and rescue

To investigate the neurological and cardiac effects linked to reduced FXN levels and to create a model for testing new therapies *in vivo*, we sought to generate mice that develop titratable clinical and pathological features of FRDA. We employed recombinase-mediated cassette exchange for genomic integration of a single copy shRNA transgene (doxycycline-inducible) that can mediate frataxin silencing temporally under the control of the H1 promoter via its insertion in a defined genomic locus that is widely expressed (rosa26 genomic locus)[28]. This allowed us to circumvent the lethal effect of organism-wide knockout, while permitting significant frataxin reduction in all tissues. Depending on the dose of the inductor doxycycline (dox), temporal *Fxn* knockdown was achieved to control the onset and progression of the disease (**Fig. 1a**).

Six different shRNA sequences were screened in vitro to obtain a highly efficient shRNA targeting the mature coding sequence of frataxin (**Fig. 1b** and **Supplementary Fig. 1**). Transgenic animals (FRDAkd) containing a single copy of this efficient shRNA transgene (**Fig. 1b)** were generated and characterized. First, to test *Fxn* knockdown efficiency, we explored the response to dox at varying escalating doses in drinking water. At the higher doses, we observed mortality as early as two weeks and a 100% mortality rate by 5 to 6 weeks, not permitting extended time series analyses (Online Methods). We found that the combination of 2 mg/ml in drinking water coupled with 5 or 10 mg/kg intraperitoneal injection of dox twice per week, led to efficient *Fxn* knockdown within two weeks post treatment initiation, while avoiding a high early mortality rate (Online Methods). Hence, for all subsequent experiments we utilized this regimen to model the chronicity of this disorder in patients by balancing the gradual appearance of clinical signs and decline in function, while limiting early demise (**Fig. 1c**).

To determine the effect of *Fxn* deficiency in adult mice after a period of normal development (similar to a later onset phenotype in humans), which would allow establishment of stable baselines, and to obtain relatively homogeneous data from behavioral tests[29] we initiated dox at 3 months. Following twenty weeks with (Tg +) or without (Tg -) doxycycline administration (**Fig. 1c;** Online

Methods), we observed highly efficient silencing of *Fxn*, reaching greater than 90% knockdown across multiple CNS and non-CNS tissues ($P < 0.05$, two-way ANOVA; **Fig. 1d,e**). Using this regimen, time series western blot analyses of 80 independent animals (wildtype with dox (Wt +) N= 24; transgenic with dox (Tg +) N= 24; transgenic without dox (Tg -) N= 24; transgenic with dox removal (Rescue Tg ±) N= 8, at weeks 0, 3, 8, 12, 16 and 20) confirmed efficient silencing as early as 3 weeks, and efficient rescue, as evidenced by normal frataxin levels, post 8 weeks dox removal ($P < 0.05$, two-way ANOVA; **Fig. 1f,g**). Together, the results indicate that FRDAkd mice treated with dox are effectively FXN depleted in a temporal fashion and that *Fxn* expression can be reversed efficiently by dox removal, making it suitable for studying pathological and clinical phenotypes associated with FRDA.

Frataxin knockdown mice exhibit neurological deficits

The major neurologic symptom in FRDA is ataxia, which in conjunction with other neurological deficits including axonal neuropathy and dorsal root ganglion loss, contributes to the gait disorder and neurological disability[8,9]. So, we first determined whether *Fxn* knockdown impacted the behavior of Tg and Wt mice with (+) or without (-) dox, or with dox, followed by its removal (±; the "rescue" condition), leading to a total of five groups subjected to a battery of motor behavioral tasks (each group N = 15-30; total mice = 108; Online Methods) (**Fig. 2a-g)**. Wt - and Wt + control groups were included to access baseline and to have a control for any potential dox effect on behavior; Tg - and Tg + transgenic groups were compared to examine the effect of genotype and *Fxn* knockdown on behavior; The Tg ± group was included to study the effect of FXN restoration after knockdown (rescue). We observed significant weight loss and reduced survival ratio (<90%) at 25 weeks with dox treatment in *Fxn* knockdown animals (Tg +) when compared to other control groups ($P < 0.05$, two-way ANOVA; **Fig. 2a**,**b**). Tg + mice exhibited a shorter distance travelled at both 12 and 24 weeks in comparison to control animals, consistent with decreased locomotor activity ($P < 0.05$, two-way ANOVA; **Fig. 2c**). Next, we assessed gait ataxia[9] using paw print analysis[30] (Online Methods). The *Fxn* knockdown mice (Tg +) displayed reduced hind and front limb stride length when compared with Tg-, as well as the Wt control + and - dox

at 12 and 24 weeks, suggesting ataxic gait ($P < 0.05$, two-way ANOVA; **Fig. 2d,e** and **Supplementary Fig. 2**). Grip strength testing also showed that Tg + animals displayed defect in their forelimb muscular strength at 12 and 24 weeks when compared with other groups ($P < 0.05$, two-way ANOVA; **Fig. 2f**). Finally, motor coordination and balance were evaluated using the Rotarod test. Whereas no significant difference in time spent on the rod before falling off was seen between Wt + or Wt - or Tg - and Tg ± mice after 12 weeks post dox removal (rescue), chronically treated mice (Tg + mice) from 12 weeks onward fell significantly faster, indicative of motor impairments ($P < 0.05$, two-way ANOVA; **Fig. 2g**). These observations suggest that the knockdown of *Fxn* in mice causes motor deficits indicative of ataxia similar to FRDA patients[9], and demonstrates the necessity of normal levels of *Fxn* expression in adults for proper neurological function.

Frataxin knockdown leads to cardiomyopathy

Cardiac dysfunction is the most common cause of mortality in FRDA[31,32]. To examine impaired cardiac function in FRDAkd knockdown animals, we employed electrocardiogram (ECG) and echocardiogram analyses to measure electrical activity and monitor cardiac dimensions. The ECG of Tg + mice displayed a significant increase in QT interval duration when compared to the other control/comparison groups at both 12 and 24 weeks post dox treatment, suggesting abnormal heart rate and rhythm (arrhythmia)[33] (Online Methods; $P < 0.05$, two-way ANOVA; **Fig. 3a,e**). However, rescue animals (Tg ±) 12 weeks after dox removal showed normal electrocardiogram, demonstrating that by restoring the FXN levels, the prolonged QT interval can be reversed ($P < 0.05$, two-way ANOVA; **Fig. 3b,e**). We also observed that the Tg + animals at week 24 displayed absence of P-waves suggesting an atrial conduction abnormality[34] (**Fig. 3c**), not observed in the rescued animals. Similar abnormalities have been variably observed in many FRDA patients[35].

Progressive hypertrophic cardiomyopathy (thickening of ventricular walls) related to the severity of frataxin deficiency[35-37] is frequently observed in FRDA patients[31]. To confirm structural cardiac abnormalities, echocardiogram analyses were performed, focusing on left ventricular function. At 12 weeks there was a non-significant trend towards increasing ventricular wall thickness. However, by 24

weeks, dox treated transgenic animals (Tg +) exhibited ventricular and posterior wall thickening, suggesting hypertrophic cardiomyopathy in these animals when compared to other control groups ($P < 0.05$, two-way ANOVA; **Fig. 3d,f,g**). Together, these observations indicate that the transgenic mice exhibit progressive cardiomyopathy due to reduced level of *Fxn*, supporting the utilization of Tg + mice for examining the molecular mechanisms downstream of *Fxn* deficiency responsible for cardiac defects.

Cardiac pathology observed with frataxin knockdown

We next explored pathological consequences of FRDA knockdown in FRDAkd mice. In FRDA patients, reduced frataxin induces severe myocardial remodeling, including cardiomyocyte iron accumulation, myocardial fibrosis and myofiber disarray[9]. Indeed, we observed substantially increased myocardial iron in Tg + mice, as evidenced by increased ferric iron staining (**Fig. 4a** and **Supplementary Fig. 3**) and the increased expression of iron metabolic proteins, ferritin and ferroportin at 20 weeks (**Fig. 4b** and **Supplementary Fig. 3**). Cardiac fibrosis is commonly found in association with cardiac hypertrophy and failure[38]. Histological analysis by Masson's trichrome staining revealed excessive collagen deposition in Tg + mice hearts at 20 weeks when compared to other control groups, suggesting cardiac fibrosis (**Fig. 4c**). Further examination of cardiomyocyte ultrastructure by electron microscopy in control mouse (Wt +) heart demonstrates normally shaped mitochondria tightly packed between rows of sarcomeres (**Fig. 4d**). In contrast, Tg + mice demonstrate severe disorganization, displaying disordered and irregular sarcomeres with enlarged mitochondria at 20 weeks (**Fig. 4d**). In a minority of cases, but never in controls, we observed mitochondria with disorganized cristae and vacuoles in Tg + mouse heart at 20 weeks, suggesting mitochondrial degeneration (**Fig. 4e**). Next, by examining aconitase which is a Fe-S containing enzyme whose activity is reduced in FRDA patients[39,40], activities in Tg + and other control groups, we observed decreased aconitase activity in the Tg + mouse heart at 20 weeks. Together these observations suggest that the knockdown of *Fxn* in mice causes cardiac pathology similar to that observed in patients[32].

Frataxin knockdown causes neuronal degeneration

In FRDA patients and mice with *Fxn* conditional knockout, a cell population that is seriously affected by frataxin reduction is the large sensory neurons of dorsal root ganglia (DRG), which results in their degeneration[9]. As in heart tissue, lack of *Fxn* also induces mitochondrial dysfunction in the DRG[40]. Thus, we assessed whether mitochondrial abnormalities are observed in Tg + mice DRG neurons by electron microscopy (Online Methods). As anticipated, no mitochondrial abnormalities were detected in DRG neurons in control groups, but a significant increase ($P < 0.05$, two-way ANOVA) in condensed mitochondria were detected in DRG neurons of Tg + mice at 20 weeks (**Fig. 5a-c,e**), but not in Tg - or Wt + mice. In most cases we observed lipid-like empty vacuoles associated with condensed mitochondria in DRG neurons of Tg + animals, but not in other control groups, suggesting neuronal degeneration, similar to what is observed in FRDA patients[9] ($P < 0.05$, two-way ANOVA; Online Methods; **Fig. 5b,c**). Previous results in human post-mortem spinal cords of FRDA patients showed a decrease in axon size and myelin fibers[8]. By analyzing more than 2000 axons per group in the lumbar spinal cord cross-section of high-resolution electron micrographs, we observed significant reduction in axonal size and myelin sheath thickness in the spinal cord samples of Tg + mice when compared to other control groups at 20 weeks ($P < 0.05$, two-way ANOVA; **Fig. 5f,g**). In the cerebellum, the number of Purkinje cells, the cerebellar granular and molecular layers were not altered due to *Fxn* knockdown at 20 weeks (**Supplementary Fig. 4**).

Next we explored the visual system, because in FRDA patients, various visual field defects have been reported, suggesting that photoreceptors and the retinal pigment epithelium (RPE) can be affected[41,42]. By electron microscopic examination of the photoreceptors in the retina, which are specialized neurons capable of phototransduction, we observed disruption in Tg + mice at 20 weeks (Online Methods; **Fig. 5h**). Previous work has shown that the disruption of photoreceptors is related to visual impairment[43]. Similarly, we also found a significant increase in degenerating RPE cells with vacuoles in Tg + mice, which is involved in light absorption and maintenance of visual function (**Fig. 5i**). Together, these results suggest that *Fxn* knockdown in the CNS of adult mice results in degeneration of retinal neurons.

Gene expression changes due to frataxin knockdown

Given the phenotypic parallels in the cardiac and nervous system abnormalities in FRDAkd mice with chronic *Fxn* reduction following treatment with dox, we next sought to explore genome wide molecular mechanisms and determine which pathways were affected in the heart and nervous system, and if they were reversible. We analyzed global gene expression profiles in the heart, cerebellum and DRGs from Tg +, Tg -, Wt + and Tg ± mice from 0, 3, 12, 16, 20 and plus 4, 8 weeks post dox treatment (n= 192). Differential expression analyses (Online Methods) identified 1959 genes differentially expressed in Tg + mice heart when compared to Wt + and Tg - mice (FDR < 5%, **Fig. 6a, Supplementary Table 1**). Similarly, we observed 709 and 206 genes differentially expressed in cerebellum and DRGs of Tg + mice. While cross tissue overlap in expression changes was significant, the majority of changes were tissue specific; only 31% and 38% of genes that were differentially expressed in the Tg + mice cerebellum and DRGs were also dysregulated in heart. Likewise, we observed a 19% overlap between DRGs and cerebellum, consistent with previous observations that *Fxn* reduction causes distinct molecular changes in different tissues[15].

Next, we analyzed these differently expressed transcripts in cardiac tissue from Tg + mice with respect to cellular pathways. The top GO categories and KEGG pathways include chemotaxis, immune response, lysosome and phagocytosis, vesicle transport and endocytosis, p53 signaling pathway, cell cycle and division, protein transport and localization, nucleoside and nucleotide binding, and mitochondrion (Benjamini corrected P-value < 0.05) (**Fig. 6a, Supplementary Table 2**). To characterize the temporal patterns of these signaling cascades after frataxin knockdown and rescue, we examined their time course by PCA analyses of the gene expression profiles (**Fig. 6b**). By examining the cumulative explained variability of the first three principal components for these clusters of genes, we show that each of these functional groups are activated as early as three weeks after dox initiation (and remain elevated for up to 20 weeks); importantly, the aberrant expression of all of these clusters observed in Tg + mice are largely reversed after eight weeks of rescue via *Fxn* re-expression (**Fig. 6a,b**).

Another notable observation is that immune system activation is among the earliest pathways regulated after *Fxn* knockdown (**Fig. 6b**). This suggests that initiation of immune responses (innate and adaptive) is a direct consequence of *Fxn* knockdown. For example, 38 genes involved in the chemokine signaling pathway (KEGG: mmu04062) were significantly differentially expressed due to *Fxn* knockdown in Tg + mice heart (**Supplementary Fig. 5**). Cross validating these genes with previously published gene expression datasets obtained from FRDA patients[44] and mouse models associated with FRDA[20,23], identified several genes involved in the chemokine signaling pathway (E.g.: CCL2, 3, 4, 7, CXCL1, 16, PRKCD, STAT3) consistently differentially expressed in these six independent FRDA associated datasets (**Supplementary Fig. 6**). This implicates a vital role for chemokines and immune response in FRDA pathology, as has been suggested for other neurodegenerative diseases[45-48].

Shared and tissue specific gene expression changes

We next performed weighted gene co-expression network analysis (WGCNA)[49-51], a powerful method for understanding the modular network structure of the transcriptome, to organize the frataxin related transcriptional changes in an unbiased manner following knockdown and rescue. WGCNA permits identification of modules of highly co-expressed genes whose grouping reflects shared biological functions and key functional pathways, as well as key hub genes within the modules, and has been widely applied to understanding disease related transcriptomes[52,53]. By applying WGCNA and consensus network analysis[50] we identified 19 robust and reproducible co-expression modules (Online Methods; **Supplementary Fig. 7 and Supplementary Table 3**) between the three tissues datasets generated at 0, 3, 12, 16 and 20 weeks after *Fxn* knockdown and 4 and 8 weeks post dox removal. On the basis of the module eigengene correlation with time-dependent changes after *Fxn* knockdown, we first classified modules as up-regulated and down-regulated following knockdown (**Supplementary Fig. 8**). Next, based on the significant module trait relationships (Wilcoxon P-value < 0.05), we identified 11 modules strongly associated with *Fxn* knockdown: three down-regulated modules in two or more tissues after *Fxn* knockdown (yellow, lightgreen and turquoise) and three up-regulated modules (blue,

purple, and black) (**Supplementary Fig. 8**), three down-regulated modules in heart, which were up-regulated in cerebellum (red, greenyellow and magenta) and two up-regulated modules in heart which were down-regulated in cerebellum (cyan and pink). Although six of the gene co-expression modules (yellow, lightgreen, turquoise, blue, purple, and black) in the heart, cerebellum and DRG following *Fxn* knockdown are highly preserved across tissues, five modules (red, greenyellow, magenta, cyan and pink) exhibit differential expression profiles suggesting tissue specific molecular changes, consistent with previous observations of shared and organ specific changes[15] (**Supplementary Fig. 8**).

As a first step toward functional annotation of the cross tissue modules, we applied GO and KEGG pathway enrichment analyses, which showed enrichment (Benjamini-corrected p values < 0.05) for several GO categories and pathways in the *Fxn* knockdown co-expression modules which included several previously associated functional categories related with FRDA (**Supplementary Table 4**). Three modules (yellow, lightgreen and turquoise) that were down-regulated in two or in all three tissues due to *Fxn* knockdown included, nucleotide, nucleoside and ATP binding, myofibril assembly, muscle tissue development, RNA processing, and several mitochondrial related categories: oxidative phosphorylation, respiratory chain, NADH dehydrogenase activity, and electron transport chain. We also observed that the genes present in turquoise module were enriched for several KEGG pathways, namely, PPAR signaling (mmu03320; genes=14), insulin signaling (mmu04910; n=19), fatty acid metabolism (mmu00071; n=10), cardiac muscle contraction (mmu04260; n=20), dilated cardiomyopathy (mmu05414; n=13), and hypertrophic cardiomyopathy (mmu05410; n=14), which have been previously associated with FRDA, reflecting the multi-systemic nature of FRDA. Similarly, three upregulated cross tissue modules (blue, purple, and black) include, nucleotide binding, vesicle-mediated transport, immune response (innate and adaptive), defense response, inflammatory response, induction of apoptosis, positive regulation of cell death, cell adhesion, and skeletal system development (**Supplementary Table 4**). These results demonstrate that unsupervised analyses can identify groups of genes not only with shared biological functions, but also relevant to the clinical phenotypes observed in FRDA.

Three tissue specific modules that were down-regulated in heart and up-regulated in cerebellum (red, greenyellow and magenta) showed enrichment for, transcription regulator activity, neurological system process, synaptic vesicle and nucleotide, nucleoside and ATP binding. Two other modules that were up-regulated in heart and down-regulated in cerebellum (cyan and pink) were enriched for cell cycle, cell division, mitosis and DNA replication (**Supplementary Table 4**). In summary, we observed several metabolic functional categories that were differentially expressed (up and down) due to *Fxn* knockdown. The modules consisting of mitochondrial and cardiac specific categories along with PPAR signaling, insulin signaling, fatty acid metabolism pathways were down regulated in all tissues. Likewise, the modules enriched for immune, apoptosis and cell death related categories we up-regulated in all tissues due to *Fxn* knockdown. Synaptic and transcription regulator activity functional categories were only up-regulated in cerebellum, whereas cell cycle, cell division, mitosis and DNA replication related functional categories were down-regulated in cerebellum and up-regulated in the heart. These general functional categories related to *Fxn* knockdown have been previously associated with altered function in FRDA patients[44,54], suggesting that genes within these modules would make interesting candidate genes for follow up studies, because many of the genes have not been previously associated with FRDA pathology and the disease mechanism.

Gene expression candidate biomarkers associated with frataxin knockdown

To identify candidate molecular targets and to better understand the molecular mechanism associated with *Fxn* knockdown, we first manually combined all the GO ontology terms (see above and **Supplementary Table 4**) that were enriched in the 11 modules into 26 broad functional categories based on GO slim hierarchy (**Supplementary Table 5**) and screened for co-expressed genes within each functional category in all three tissues ($r > 0.5$ and P-value < 0.05) over the time course. This allowed us to identify critical functional sub-categories that are up or down regulated due to frataxin knockdown and subsequently permitted us to detect differentially expressed candidate genes that are co-expressed within each functional category (**Fig. 6d; Supplementary Fig. 9**). For example, we show that immune, cell cycle and apoptosis related functional groups are up-regulated, whereas cardiac,

macromolecule and mitochondrial related functional groups were down-regulated (**Fig. 6d**). In the immune category, we observed most prominent changes in complement activation pathway genes, namely, C3, C4B, C1QB, C1QC and Serping1. Interesting, we also observed that many of these genes were also up-regulated in peripheral blood mononuclear cells obtained from FRDA patients (**Supplementary Fig. 10**), suggesting the potential for complement activation to act as a biomarker for FRDA as previously suggested for other degenerative diseases[55]. Similarly, we found several genes, for example, CACNA2D1, ABCC9 and HRC involved in normal cardiac function, to be down-regulated in heart tissue upon frataxin knockdown (**Fig. 6d**). CACNA2D1 is associated with Brugada syndrome, also known as sudden unexpected nocturnal death syndrome, a heart condition that causes ventricular arrhythmia[56]. Mutations in ABCC9 gene can cause dilated cardiomyopathy[57] and a genetic variant in the HRC gene has been linked to ventricular arrhythmia and sudden death in dilated cardiomyopathy[58]. These observations suggest that lower levels of frataxin causes dysregulation of multiple genes related to arrhythmia or cardiac failure, a primary cause of death in FRDA patients.

There has been accumulating evidence suggesting that apoptosis may be an important mode of cell death during cardiac failure[59]. In agreement with this, we observed genes related to apoptosis were up-regulated after *Fxn* knockdown in FRDAkd mice heart (**Fig. 6d**), which has been previously associated with FRDA pathogenesis and reported in other *Fxn* deficiency models[24,60,61]. In order to validate our network findings, we tested CASP8 protein levels[62], observing an increase in cleaved Caspase 8 protein levels in Tg + heart tissue compared with control mice (**Fig. 6e**). Next, we employed the TUNEL assay to detect apoptotic cells that undergo extensive DNA degradation during the late stages of apoptosis[63]. However, we did not observe an increase in cell death in all tissues by TUNEL staining (**Fig. 6f**).

Literature data extraction for candidate genes associated with frataxin knockdown

We next examined the phenotype-gene associations extracted by co-occurrence-based text-mining in an attempt to link FRDA disease phenotypes with genes. For this, we screened the literature for potential co-occurrence link association between the observed FRDAkd mice phenotypes and the

genes that are differentially expressed after *Fxn* knockdown (Online Methods). Identifying potential biomarker candidates that are previously validated for certain phenotypes can provide insight into disease progression, pathogenesis and extremely valuable for assessing therapeutic options[64]. We screened with the genes that are differentially expressed (FDR < 5%) and present in the co-expression modules associated with behavioral and pathological key-terms (Eg: ataxia; **Supplementary Table 6**) in the published literature. Interestingly, this analysis identified numerous genes in which mutations are known to cause Mendelian forms of ataxia namely, ANO10[65,66], CABC1[67,68] and POLG[69,70] that were significantly down-regulated in the heart tissue and mildly down-regulated in the cerebellum after *Fxn* knockdown in Tg + animals (**Fig. 6g and Supplementary Fig. 11**). We also found three other genes that are differentially expressed due to *Fxn* knockdown, namely, CSTB[71], NHLRC1[72] and PMM2[73] all of which are associated with other disorders when mutated causes ataxia (**Fig. 6g**). These observations suggest that *Fxn* along with multiple other downstream candidates causes behavioral deficits in FRDAkd mice. Similarly, for cardiac phenotypes, we identified multiple genes related to cardiac fibrosis that were up-regulated in FRDAkd mice heart (**Fig. 6g**), including LGALS3[74], ICAM1[75] and TIMP1[76] were up-regulated (**Fig. 6g**). Genes related to iron regulation, included HFE[77], SLC40A1[77], HMOX1[78], TFRC[77] and GDF15[79] all of which are directly involved in hemochromatosis and iron overload (**Fig. 6g**). We also found previously associated genes related with muscle strength (E.g.: SRL, DCN), myelination (E.g.: PMP22, LGALS3, TLR2 and SIRT2) and several genes related to neuronal degeneration (E.g.: GRN and APP) to be dysregulated in FRDAkd mice (**Fig. 6g and Supplementary Fig. 11**), connecting this degenerative disorder with the molecular signaling pathways known to be causally involved in other such disorders.

Perhaps the most prominent such known pathway associated with neurodegeneration, was autophagy, since several autophagy-related genes (LAMP2, ATF4, TLR2, OPTN, MAPK14, SIRT2, ICAM1, LGALS3, DCN, RCAN1, GRN) were present in these disease phenotype-associated sub networks (**Fig. 6g**). Disruption of autophagy is also reported as altered in other *Fxn* deficiency models[24,60,61] and is associated with various stress conditions including mitochondrial dysfunction[80,81]. Autophagy is responsible for the recycling of long-lived and damaged organelles by lysosomal

degradation[82]. To validate our network findings, we utilized LC3-II as a marker for autophagy, showing autophagy activation in Tg + mice heart, but not in spinal cord tissue (**Fig. 6e, h**). This suggests activation of apoptosis (**Fig. 6d, e**) and autophagy (**Fig. 6e, h**) may therefore potentiate the cardiac dysfunction of Tg + mice. Next, by examining the expression levels of all these sub network genes (**Fig. 6g**) in the datasets of other FRDA related mouse models and patient peripheral blood mononuclear cells, we show that they are also differentially expressed in the same direction (**Fig. 6i**), suggesting these sub network genes can be ideal candidates for molecular biomarkers in FRDA. In summary, consistent with our behavioral, physiological and pathological findings, we show multiple candidate genes related to key degeneration related phenotypes to be altered in FRDAkd mice.

Rescue of behavioral, pathological and molecular changes due to frataxin restoration

Our data show that mice carrying the dox inducible shRNA for *Fxn* develop normally until they are challenged with dox, which subsequently results in substantial FXN reduction and causes multiple behavioral and pathological features observed in patients with FRDA, including cardiac and nervous system dysfunction (**Fig. 2-5**). *Fxn* knockdown mice displayed remarkable parallels with many of the behavioral, cardiac, nervous system impairments along with physiological, pathological and molecular deficits observed in patients. At a general level FRDAkd mice displayed weight loss, reduced locomotor activity, reduced strength, ataxia and early mortality (**Fig. 2**). In the nervous system, FRDAkd mice showed abnormal mitochondria and vacuolization in DRGs, retinal neuronal degeneration, and reduced axonal size and myelin sheath thickness in the spinal cord[8,9,24,25] (**Fig. 5**). With regards to cardiac dysfunction, FRDAkd mice exhibited conduction defects, cardiomyopathy, evidence of iron overload, fibrosis, and biochemical abnormalities that are commonly observed in patients[8,9,25] (**Fig. 3,4**). These features correspond to a phenotype of substantial multisystem, clinical disability consistent with moderate to severe disease after 3 months of frataxin deficiency and that lead to a 50% mortality rate at approximately 5 months in these mice.

Given that optimal therapy in patients with FRDA could be considered replenishment of FXN itself (e.g. via gene therapy[83] or improvement of *Fxn* transcription via small molecules[84]), we next asked

how much of the behavioral, physiological, pathological and molecular phenotype(s) observed at this relatively severe stage of illness could be reversed following such “optimal” therapy. In this case, optimal therapy is return of normal FXN levels under endogenous regulation through relief of exogenous inhibition. Answering this question of reversibility is crucial for any clinical trial, whatever the mechanism of action of the therapy, since we currently have limited information as to what represents potentially reversible neurologic or cardiac phenotypes.

To address this, we compared two groups of mice, both transgenic and treated with dox for 12 weeks, at which time both groups show equivalent levels of substantial clinical features (**Supplementary Fig. 12**). In one, Tg + the dox is continued for another 12 or more weeks, and in the other Tg ± the dox is removed and the animals are followed. Restoration of FXN expression in *Fxn* knockdown mice (Tg ±) that had reached a level of substantial clinical dysfunction led to significant improvement in lifespan (no death until 20 weeks post dox removal) when compared to Tg + group which resulted in 90% mortality rate by 25 week post dox treatment (**Fig. 2b**). Rescue animals (Tg ±) also displayed rapidly improvement in: gait ataxia, body weight, muscle strength, locomotor activity, and balance on rotarod test over the ensuing 12 week period, to a point where the treated animals were not significantly different from controls on many tests (**Fig. 2**). Remarkably, we observed all of the six FRDA associated clinical phenotypes tested showed significant improvement, suggesting that FRDA-like neurological defects due to absence of the mouse *Fxn* gene can be rectified by delayed restoration of *Fxn* (**Fig. 2**).

We next sought to determine whether the observed reversible behavioral changes in FRDAkd mice are also accompanied by recovery of the physiological phenotype in FRDAkd mice heart, since, changes in physiology offer attractive therapeutic targets for symptomatic and preventive treatment of ataxia. Our results in Tg ± mice which received the dox for 12 weeks followed by 12 weeks dox removal displayed reversal of long QT interval phenotype, when compared to Tg + mice at both 12 and 24 weeks post dox treatment (**Fig. 3a,b,e**). We observed the ventricular and posterior wall thickening only at 24 weeks post dox treatment in Tg + animals (**Fig. 3d,f,g**), suggesting that long QT interval

phenotype is a prominent early manifestation of disease that occurs before left ventricular wall thickness and show that correcting this aberrant physiology through activation of *Fxn* gene expression is a potential route to therapy.

One question that intrigued us because of its striking behavioral and physiological functional recovery is to what extent these changes represented pathological findings related to cell dysfunction (potentially reversible) versus cell death (irreversible) recovery. Pathological and biochemical analyses in Tg ± mice heart at post 8 weeks dox withdrawal revealed improved cardiac function displaying reduced iron and ferritin accumulation, myocardial fibrosis, well ordered sarcomers, normal aconitase activity and reduced mitochondrial degeneration (**Fig. 4**). Relevant to the pathogenesis of FRDA heart and the role of iron and mitochondrial defect, it has been found that cells with these defects are sensitized to cellular dysfunction[85,86], and here we show this can be ameliorated by *Fxn* restoration.

In the nervous system of Tg ± mice post 8 weeks dox removal, we observed reduced vacuoles and fewer condensed, degenerating mitochondria in DRG neurons along with several abnormal mitochondria containing DRG neurons (**Fig. 5a,b,d,e**). However we only observed mild improvement in myelin sheath thickness and cross section axonal size in the spinal cord of Tg ± mice during this time period (**Fig. 5f,g**). Conversely, we observed a significant reduction in the number of vacuoles and disrupted photoreceptors in the retina of Tg ± mice, indicating that *Fxn* restoration rescued photoreceptor degeneration (**Fig. 5h,i**). These findings establish the principle of cellular dysfunction reversibility in FRDAkd mouse model due to *Fxn* restoration and, therefore, raise the possibility that some neurological and cardiac defects seen in this model and FRDA patients may not be permanent.

In line with remarkable recovery of several behavioral, physiological and pathological defects in FRDAkd mice, we also observed that the genome-wide molecular biomarker represented by gene expression analyses due to *Fxn* knockdown could be completely rescued after *Fxn* restoration (**Fig. 6**). By rescuing the FXN protein levels back to the near basal level, we were able to reverse the molecular changes completely. At post 8 weeks of dox removal after initial 12 weeks of dox treatment, we examined the number of differentially expressed genes at false discovery rate of 5% in all tissues and

observed 100% recovery of gene expression levels in cerebellum and DRGs, and 99.95 % of reversed gene expression levels in the heart of FRDAkd mice (**Fig. 6a,b**). These results which included several pathways (**Fig. 6a,c,d**) that are significantly affected due to *Fxn* depletion and complete reversal (**Fig. 6a,b**) of these pathways due to *Fxn* restoration can serve as gene-expression signature for evaluation of various therapeutic paradigm.

In summary, all six behavioral deficits in FRDAkd mice were reversed (**Fig. 2**), in the cardiac system, the long QT interval phenotype along with various pathological mainfestations including mitochondrial defects were reversed, in the nervous system, we observed improvement in DRGs and photoreceptor neurons, and complete reversal of the molecular changes in all three tissues suggesting near basal *Fxn* levels are sufficient to elevate behavioral symptoms in the preclinical FRDAkd model. The rapidity of *Fxn* expression due to dox removal and its robust correction of various parameters, even when restored after the onset of motor dysfunction, makes this FRDAkd mouse model an appealing potential preclinical tool for testing various therapeutics for FRDA.

DISCUSSION

Here we report development and extensive characterization of a novel, reversible mouse model of FRDA based on knock-down of frataxin by RNA interference[28], the FRDAkd mouse. Treated transgenic mice developed abnormal mitochondria, exhibit cardiac and nervous system impairments along with physiological, pathological and molecular deficits. These abnormalities likely contributed to the behavioral phenotype of FRDAkd mice, parallel to what is observed in FRDA patients[8,9]. Importantly, restoration of *Fxn* expression, even after the development of severe symptoms and pathological defects, resulted in a drastic amelioration of the clinical phenotype, both in the cardiac and nervous systems, including motor activity. Pathology was significantly improved in the heart, DRGs and in the retina, but only mild improvement was observed in spinal cord, suggesting *Fxn* restoration for the duration of 8 weeks is not sufficient for reversal of neuronal defects in the spinal cord after *Fxn* knockdown. Interestingly, the patterns of gene expression changes due to *Fxn* knockdown in three different tissues differed[15], indicating variable response to frataxin deficiency, which could partly explain cell and tissue selectivity in FRDA[87]. The onset and progression of the disease correlates with the concentration of doxycycline, and the phenotype returns to baseline after its withdrawal. The onset of transgene expression to achieve *Fxn* knockdown and robust recovery of symptoms due to restoration of *Fxn* levels in a mouse model of FRDA, even when reversed after the onset of the disease, makes this model an appealing potential preclinical tool for developing FRDA therapeutics. This approach will also enable new insights into FRDA gene function and molecular disease mechanisms.

Several models of FRDA have been developed and each have advantages and disadvantages[25]. This new FRDAkd model exhibits several unique features that provide advantages for the study of FRDA pathophysiology relative to other existing models[20-25]. First, induction of frataxin knockdown permits circumventing potential confounding developmental effects[19] and has the flexibility to enhance the disease onset and progression very rapidly by increasing the doxycycline dose. Moreover, the temporal control of *Fxn* knockdown can provide further insights into the sequence of tissue vulnerability during the disease progression[87]. Second, reversibility of *Fxn* knockdown provides a unique model to mimic the effect of an ideal therapeutic intervention. Along this line, it has so far not

been established to what extent FXN restoration after the onset of clinical motor symptoms is successful to prevent occurrence and/or progression of FRDA. Therefore, this model will be of central importance to gain better insights into disease pathogenesis and to test therapeutic agents. Third, the doxycycline-dependent reduction of *Fxn* expression can be tailored to carefully determine the critical threshold of *Fxn* levels necessary to induce selective cellular dysfunction in the nervous system (DRGs and spinal cord) and to understand the occurrence of tissue specific dysfunction in FRDA. Thereby, these experiments will help to understand the tissue specificity and generate clinically relevant tissue targeted therapeutics for FRDA. Finally, the temporal control of single copy and reversible regulation of shRNA expression against *Fxn* produces reproducible transgene expression from the well-characterized rosa26 locus to generate the first model to exhibit and reverse several symptoms parallel to FRDA patients. Here, we focused on the consequences of frataxin removal in an otherwise healthy adult animal. However, we should emphasize that this FRDAkd model uniquely facilitates future studies exploring prenatal or early post natal knockdown, and a wide variety of time course studies to understand disease pathophysiology and to identify potential imaging, physiological, or behavioral correlates of likely reversible or non-reversible disabilities in patients.

We show that FRDAkd animals are defective in several behaviors and exhibit weight loss, reduced locomotor activity, reduced strength, ataxia and early mortality. All of these defects were significantly improved following *Fxn* restoration, approaching or reaching wild-type levels. Most importantly ataxia and survival are well-established and important clinical endpoints in FRDA[31], readouts after *Fxn* restoration clearly improve these parameters and appear to be directly related to the functional status of the FRDAkd mice. We conclude that *Fxn* deficient mice exhibit considerable neurological plasticity even in a nervous system that is fully adult. Hence, utilizing these reversible intermediate behavioral phenotypes as biomarkers will help us determine the disease progression and test various FRDA treatment options in this model.

Hypertrophic cardiomyopathy is a common clinical feature in FRDA and approximately 60% of patients with typical childhood onset FRDA die from cardiac failure[31]. It is generally believed that cardiac failure is caused by the loss of cardiomyocytes through activation of apoptosis[88]. We observed

activation of early apoptosis pathways in heart tissue and severe cardiomyopathy characterized by ventricular wall thickness[89]. However, we did not observe TUNEL positive cells in either heart or nervous system. This may reflect that the model is in a early phase of cell death initiation, or rather that apoptotic cells are readily phagocytosed by neighbouring cells and are consequently difficult to detect[90]. We also observed enhanced activation of autophagy in the heart tissue of FRDAkd mice, where autophagic cardiomyocytes are observed at a significantly higher frequency during cardiac failure[91]. These results suggest that apoptosis and autophagy together might synergistically play a vital role in the development of cardiac defect in FRDA[92].

During *Fxn* knockdown, FRDAkd mice initially exhibited a long QT interval at 12 weeks during electrocardiographic analyses followed by the absence of P-waves and increased ventricular wall thickness at 24 weeks. Restoration of *Fxn* levels at 12 weeks reversed long QT interval phenotype. However, it will be interesting to examine if the ventricular wall thickness can be restored by a more prolonged rescue time period. Another prominent feature of *Fxn* deficiency mouse and FRDA patients is iron accumulation and deficiency in activity of the iron-sulfur cluster dependent enzyme, aconitase, in cardiac muscle[23,40,85,86]. Consistent with these observations, we observed increased iron accumulation and reduced aconitase activity in the cardiac tissue of FRDAkd mice and we demonstrate a marked reversal of both to a statistically significant extent, suggesting *Fxn* restoration is sufficient to overcome and clear the iron accumulation and reverse aconitase activity[93]. Our gene expression data revealed several genes (HFE[77], SLC40A1[77], HMOX1[78], TFRC[77] and GDF15[79]) directly involved in hemochromatosis and iron overload to be upregulated in our FRDAkd mice, all of which were rescued to normal levels by frataxin restoration. Similarly, several downregulated genes involved in normal cardiac function (CACNA2D1, ABCC9 and HRC) were rescued by *Fxn* restoration. Together, these data indicate that *Fxn* restoration in symptomatic FRDAkd mice reverses the early development of cardiomyopathy at the molecular, cellular and physiological levels.

Cellular dysfunction due to FXN deficiency is presumed to be the result of a mitochondrial defect, since FXN localizes to mitochondria[93-95] and deficiencies of mitochondrial enzymes and function have been observed in tissues of FRDA patients[40,96]. Here we show that FRDAkd mice displayed

accumulation of damaged mitochondria, and reduced aconitase as a direct consequence of frataxin deficiency in heart, consistent with previous findings in conditional FRDA mouse models[23,24], suggesting frataxin deficiency inhibits mitochondrial function leading to cellular atrophy[97]. Restoration of FXN resulted in improvement in pathological mitochondrial structure indicating that FXN restoration prevents mitochondrial defects and may thereby enhance cell survival[93]. Our observation of mitochondrial dysfunction recovery as early as eight weeks after FXN restoration is consistent with the highly dynamic nature of mitochondria[98].

In the nervous system, we observed higher level of condensed mitochondria in DRGs through ultrastructural analyses. Condensed mitochondria are known to have lower respiratory control and ATP production[99]. On most occasions these condensed mitochondria in DRG neurons of FRDAkd mice were associated with lipid-like bodies, consistent with the known close association of lipid bodies with mitochondria observed in a variety of cell types[100]. Of particular interest, it has been shown that the junctions between these two organelles expand with an increased need for energy, suggesting the direct flow of fatty acids from lipid bodies to the mitochondrial matrix for β-oxidation to meet the cell's energy needs[101]. We observed reduced condensed mitochondria and their association with lipid-like bodies in rescue animals, suggesting that a substantial fraction of dysfunctioning frataxin-deficient mitochondria containing neurons are still viable after the onset of disease and that their dysfunction can be reversed. In the spinal cord, we observed reduction of axonal size and myelin sheath thickness in FRDAkd animals, however after eight weeks of rescue period by FXN restoration, we observed limited improvement, suggesting more time may be necessary for improved nervous system recovery. Conversely, disruption of photoreceptor neurons and degenerating RPE cells in the retina displayed robust recovery, indicating an overall morphological improvement in retinal neurons upon FXN restoration to normal levels. These findings extend previous studies showing that many defects in FRDA cells in vitro and cardiac function in vivo may be reversible following reintroduction of FXN[102] by pharmacological interventions targeting aberrant signaling processes[103] or by reintroduction of FXN by gene therapy[83].

Improved understanding of the mechanism by which FXN deficiency leads to the various phenotypes observed in FRDA is a major goal of current research in this disorder. In this regard, gene expression analyses identified several pathways altered, including, PPAR signaling pathway, insulin signaling pathway, fatty acid metabolism, cell cycle, protein modification, lipid metabolism, and carbohydrate biosynthesis, all of which have been previously associated with altered function in FRDA patients[15,54,104]. We also observed several immune components, namely, complement and chemokine cascade genes being upregulated, may be implicated as a protective mechanism after *Fxn* knockdown, and in a causal role through chronic activation of the inflammatory response[105,106]. It will be interesting to validate these genes and pathways as potent candidate biomarkers for FRDA at several stages during the disease progression.

Determining definitively whether the global expression changes observed in this study are primary or secondary to *Fxn* knockdown will require further investigation by examining dense time points immediately after *Fxn* knockdown and rescue, but our data clearly support the utility of induced models of severe disease, whereby the consequences of gene depletion can be more cleanly controlled to examine the molecular changes[28]. Together with post-induction rescue, this study highlights potential biomarkers and pathways of FRDA progression. For FRDA clinical trials, it will be important to assess whether these expression changes are translatable to the human disease and extend to other tissues that are more easily accessible than CNS or cardiac tissue. Together, these observations suggest that this work also provides a functional genomics foundation for understanding FRDA disease mechanism, progression and recovery.

In conclusion, our study provides multiple lines of evidence that *Fxn* knockdown in adult mice leads to several symptoms parallel to FRDA patients. By restoring FXN levels we show reversal of several symptoms even after significant motor defect, demonstrating the utility of this attractive model for testing potential therapeutics, such as gene therapy[83], protein replacement therapy[102], enhancement of mitochondrial function[107] and small molecules[108,109]. In fact, our findings suggest that such approaches may not only enhance FXN expression and rescue downstream molecular changes, but

may too alleviate pathological and behavioral deficits associated with FRDA, depending on the stage of the disorder.

METHODS

Methods and any associated references are available in the online version of the paper.

Accession codes. Gene Expression Omnibus: Datasets generated and analyzed in this study are available at GEO accession: GSE98790.

ACKNOWLEDGMENTS

We gratefully acknowledge support from the Friedreich's Ataxia Research Alliance to D.H.G. and V.C. (including a New Investigator Award to V.C.), and the Dr. Miriam and Sheldon G. Adelson Medical Research Foundation to D.H.G.. We thank Marianne Cilluffo for assistance with electron microscopy at the BRI Electron Microscopy Core Facility at UCLA.

AUTHOR CONTRIBUTIONS

V.C. and D.H.G. designed the experiments and wrote the manuscript. K.G., R.V., H.D., and V.C. performed the behavioral, pathological, biochemical and molecular experiments. V.C. conducted or coordinated all the experiments discussed in this manuscript with input from D.H.G.. V.S. performed network analyses and V.C. performed all subsequent bioinformatic analyses. M.J. and V.C. conducted and coordinated electrocardiogram and echocardiogram analyses. All authors discussed the results and provided comments and revisions on the manuscript.

Figure Legends

Figure 1: Efficient temporal in vivo frataxin knockdown and rescue. (**a**) Schematic representation of the inducible vector system to mediated expression of shRNA expression against frataxin. The vector contains shRNA sequence against frataxin (*Fxn*) gene regulated by the H1 promoter with tet-operator sequences (tetO) and tet repressor (tetR) under the control of the CAGGS promoter. Transcription of the *Fxn* shRNA is blocked in cells expressing the tetR. Upon induction by doxycycline (dox), tetR is removed from the tetO sequences inserted into the promoter, allowing transcription of shRNA against *Fxn*. shRNA expression leads to RNAi-mediated knockdown of *Fxn* gene. (**b**) Predicted minimum free energy secondary structure of expressed shRNA targeting the *Fxn* is shown with the sequence (sense strand) and its complement sequence (antisense strand) in the duplex form along with hairpin loop. (**c**) Timeline for doxycycline treatment of mice with a double IP injection (5 and 10 mg/kg) of dox per week and in drinking water (2 mg/ml). IP injections and dox in water was withdrawn for rescue animals. Arrow signs indicated different time intervals considered for downstream analyses. (**d**) Transgenic mice without (Tg -) or with (Tg +) doxycycline treatment (see c) for 20 weeks were analyzed by Western blot for protein levels of FXN in various organs. (**e**) For quantification, FXN values were normalized to the level of b-tubulin in each lane. (**f**) Time series FXN knockdown and rescue in liver. Wild-type mice with dox (Wt +), transgenic mice with (Tg +) and without (Tg -) dox, and transgenic mice with (Tg ±) dox removal (rescue) samples were analyzed for week 0,3,8,12,16 and 20. Rescue animals (Tg ±) were given dox for 12 weeks and doxycycline was withdrawn for additional 4 and 8 weeks. (**g**) For quantification, FXN values were normalized to the level of b-tubulin in each lane. N=4 animals per group, *=p<0.01; two-way ANOVA test; n.s., not significant. Error bars represent mean ± SEM for panels e and g.

Figure 2: Neurological deficits due to frataxin knockdown. Body weight, survival, open field, gait analysis, grip strength and rotarod in five groups of animals; wild-type mice with dox (Wt +, n= 16(WK

0), n= 16(WK 12), n= 16(WK 24)) and without dox (Wt -, n= 16(WK 0), n= 16(WK 12), n= 16(WK 24)), transgenic mice with dox (Tg +, n= 30(WK 0), n= 21(WK 12), n= 15(WK 24)) and without dox (Tg -, n= 16(WK 0), n= 15(WK 12), n= 15(WK 24)), and transgenic mice with dox removal (Tg ± Rescue, n= 30(WK 0), n= 21(WK 12), n= 20(WK 24)). (**a**) Body weight from before 6 weeks and upto 34 weeks after dox treatment. (**b**) Survival was significantly declined in dox treated Tg + group of animals, no mortality was observed after dox withdrawal (Tg ± Rescue). (**c**) Open field test showing significant decline in total distance traveled by the dox treatment transgenic animals (Tg +) at 12 and 24 weeks when compared across all other groups. After dox withdrawal, there were no differences between the rescue group (Tg ± Rescue) and the three control groups at week 24. (**d**) Gait footprint analysis of all five groups of mice at 0, 12 and 24 weeks was evaluated for stride length. Dox treated transgenic (Tg +) animals revealed abnormalities in walking patterns displaying significantly reduced stride length, however the rescue group (Tg ± Rescue) displayed normal stride length when compared to other groups. (**e**) Representative walking footprint patterns. (**f**) Grip-strength test, dox treated transgenic (Tg +) mice had reduced forelimb grip strength at 12 and 24 weeks when compared across all other groups. After dox withdrawal, there were no significant differences between the rescue group (Tg ± Rescue) and the three control groups at week 24. (**g**) Rotarod test in mice upto 34 weeks after dox treatment. Dox treated transgenic (Tg +) animals stayed less time on the rotarod than the control groups, although after dox withdrawal, there was no significant difference between the rescue group (Tg ± Rescue) and the three control groups. Values between all five groups are shown as mean ± SME. Two-way ANOVA test *=P≤0.001; n.s., not significant.

Figure 3: Frataxin knockdown mice exhibit signs of cardiomyopathy. (**a**) Representative traces of ECG recording in a wild-type and transgenic animal after dox treatment for 20 weeks, showing long QT intervals in Tg + animal. (**b**) ECG recording of a same dox treated transgenic (Tg +) animal at 12 and after dox withdrawal for additional 12 weeks (Tg ± Rescue), showing normal QT interval. (**c**) ECG recording of a same dox treated transgenic (Tg +) animal at 12 and 24 weeks, showing absences of P-

wave only at 24 week. (**d**) Representative echocardiograms from the left ventricle of a wild-type and transgenic mouse at 24 week after dox treatment. (**e-f**) Quantification of observed QT interval (**e**), ventricular septal wall thickness (**f**) and posterior wall thickness (**g**) are shown for week 12 and 24.

Figure 4: Cardiopathology of frataxin knockdown mice. (**a**) Gomori's iron staining and quantification of iron deposition in dox treated transgenic (Tg +), wild-type (Wt +) and dox withdrawn transgenic (Tg ± Rescue) animals. Dox treated transgenic (Tg +) mice showing myocardial iron-overload (a) also displayed altered expression of ferritin protein (**b**) which is involved in iron storage. Both iron-overload and ferritin protein levels were significantly lower in Tg ± Rescue animals (a-b). (**c**) Masson's trichrome staining and quantification showing increased fibrosis in Tg + mice when compared to Wt + and Tg ± Rescue animals. (**d**) Electron micrographs of cardiac muscle from Wt +, Tg + and Tg ± Rescue animals at 20 week after dox treatment. Double arrow lines indicate sarcomere. m = mitochondria. Scale bars, 1 μm. Data are representative of three biological replicates per group. (**e**) Higher magnification of electron micrographs of cardiac muscle from Tg + mice, showing normal (m) and degenerating mitochondria (asterisks). (**f**) Aconitase activity was assayed in triplicate in tissues removed from 3 hearts in each group. Values represent mean ± SME. One-way ANOVA test *=P≤0.05.

Figure 5: Frataxin knockdown mice exhibit neuronal degeneration. (**a**) Electron microscopic analysis of Wt +, Tg + and Tg ± Rescue animal DRG neurons at 20 week after dox treatment. Arrows indicate condensed mitochondria with lipid-like empty vacuoles. Insert in Tg + panel shows higher magnification of electron micrographs of condensed mitochondria with lipid-like empty vacuoles in DRG neurons. Insert in Tg ± Rescue panel shows higher magnification of abnormal mitochondria (asterisks). Nu= nucleus. (**b**) Higher magnification of electron micrographs of Tg + and Tg ± Rescue animal DRG neurons at 20 week after dox treatment. Tg + panel shows degenerating mitochondria and condensed mitochondria with lipid-like empty vacuoles in DRG neurons. Tg ± Rescue panel shows two DRG

neurons, one consisting of normal mitochondria (insert) and the other neuron with abnormal mitochondria (insert). (**c**) Higher magnification of Tg + animals showing condensed mitochondria with lipid-like empty vacuoles in DRG neurons. (**d**) Higher magnification of Tg ± rescue animals showing two DRG neurons, one consisting of normal mitochondria (normal DRG) and the other neuron with abnormal mitochondria (affected DRG). NM= normal mitochondria, CM= condensed mitochondria, EV= lipid-like empty vacuoles, AM= abnormal mitochondria. (**e**) Quantification of altered mitochondria in DRG neurons. Values represent mean ± SME. Two-way ANOVA test *=P≤0.05. (**f**) Electron micrographs of spinal cord axon cross-section, displaying reduced myelin sheath thickness and axonal cross-section area in Tg + and Tg ± Rescue animals. Bottom panel shows representative area utilized for quantification. (**g-h**) Quantification of myelin sheath thickness and axonal cross-section area in the spinal cord. Values represent mean ± SME. One-way ANOVA test *=P≤0.05. (**i**) Electron micrographs of rod and cone photoreceptor cells, showing their disruption in Tg + animals (asterisks). (**j**) Retinal pigment epithelium cell layer showing the presences of large vacuoles (arrows) in Tg + animals along with disruption in their photoreceptor cells (asterisks).

Figure 6: Gene expression analysis of frataxin knockdown mice. (**a**) Heat map of significantly up- and down-regulated genes (rows) in heart tissue of Tg + mice from 0, 3, 12, 16, 20 and plus 4, 8 weeks post dox treatment relative to controls are grouped into 13 functional categories. (**b**) Summary of differentially expressed genes during *Fxn* knockdown and rescue in heart, cerebellum and DRG tissues. (**c**) Cumulative percent of variability in Tg + gene expression data explained by the first three principal component for each functional category. (**d**) Networks highlighting differentially expressed genes due to *Fxn* knockdown in Tg + mice for selected functional categories. Nodes represents genes and edges are present between nodes when their gene expression correlation is greater than 0.5. Node size and color (red= up-regulation and green= down-regulation) denotes extent of differential expression. (**e**) Western blot analyses of Caspase 8, FXN and LC3 following 20 weeks with or without dox treatment in heart. (**f**) TUNEL assay of heart, spinal cord and DRG neurons at 20 weeks after dox treatment in Tg + mice. (**g**) Literature associated gene networks highlighting differentially expressed

genes due to *Fxn* knockdown in Tg + mice for selected key-terms. Nodes represents genes which has pairwise correlation greater than 0.5 with *Fxn* gene and edge size represents strength of their gene expression correlation. Node size correspond to number of PubMed hits with co-occurrence of gene and its corresponding key-term. Node color represents up-regulated (red) and down-regulated (green). (**h**) Representative images and quantification of LC3 staining in heart tissue at 20 weeks after dox treatment. Values represent mean ± SME. One-way ANOVA test *=P≤0.05. (**i**) Heat map depicting expression of key genes (rows) across samples (columns) for seven groups (red corresponds to gene up-regulation and blue to down-regulation). Seven groups represents, (i) ataxia, (ii) cardiac fibrosis, (iii) excess iron overload, (iv) muscular strength, (v) myelin sheath, (vi) neuronal degeneration and (vii) autophagy related genes. Column represents, seven independent datasets obtained from, FRDAsh mice, cardiac specific knockout mice[23], knock-in knockout mice[20], knock-in mice[20] and patient peripheral blood mononuclear cells[44].

References:

1. Chamberlain, S., *et al.* Mapping of mutation causing Friedreich's ataxia to human chromosome 9. *Nature* **334**, 248-250 (1988).
2. Campuzano, V., *et al.* Friedreich's ataxia: autosomal recessive disease caused by an intronic GAA triplet repeat expansion. *Science* **271**, 1423-1427 (1996).
3. Campuzano, V., *et al.* Frataxin is reduced in Friedreich ataxia patients and is associated with mitochondrial membranes. *Human molecular genetics* **6**, 1771-1780 (1997).
4. Filla, A., *et al.* The relationship between trinucleotide (GAA) repeat length and clinical features in Friedreich ataxia. *American journal of human genetics* **59**, 554-560 (1996).
5. Montermini, L., *et al.* Phenotypic variability in Friedreich ataxia: role of the associated GAA triplet repeat expansion. *Annals of neurology* **41**, 675-682 (1997).
6. Andermann, E., *et al.* Genetic and family studies in Friedreich's ataxia. *The Canadian journal of neurological sciences. Le journal canadien des sciences neurologiques* **3**, 287-301 (1976).
7. Harding, A.E. Friedreich's ataxia: a clinical and genetic study of 90 families with an analysis of early diagnostic criteria and intrafamilial clustering of clinical features. *Brain : a journal of neurology* **104**, 589-620 (1981).
8. Koeppen, A.H. & Mazurkiewicz, J.E. Friedreich ataxia: neuropathology revised. *Journal of neuropathology and experimental neurology* **72**, 78-90 (2013).
9. Koeppen, A.H. Friedreich's ataxia: pathology, pathogenesis, and molecular genetics. *Journal of the neurological sciences* **303**, 1-12 (2011).
10. Bhidayasiri, R., Perlman, S.L., Pulst, S.M. & Geschwind, D.H. Late-onset Friedreich ataxia: phenotypic analysis, magnetic resonance imaging findings, and review of the literature. *Archives of neurology* **62**, 1865-1869 (2005).
11. Li, Y., *et al.* Expanded GAA repeats impede transcription elongation through the FXN gene and induce transcriptional silencing that is restricted to the FXN locus. *Human molecular genetics* **24**, 6932-6943 (2015).
12. De Michele, G. & Filla, A. Movement disorders: Friedreich ataxia today-preparing for the final battle. *Nature reviews. Neurology* **11**, 188-190 (2015).
13. Martinez, A.R., *et al.* Nonneurological Involvement in Late-Onset Friedreich Ataxia (LOFA): Exploring the Phenotypes. *Cerebellum* (2016).
14. Galea, C.A., *et al.* Compound heterozygous FXN mutations and clinical outcome in friedreich ataxia. *Annals of neurology* **79**, 485-495 (2016).
15. Coppola, G., *et al.* Functional genomic analysis of frataxin deficiency reveals tissue-specific alterations and identifies the PPARgamma pathway as a therapeutic target in Friedreich's ataxia. *Human molecular genetics* **18**, 2452-2461 (2009).
16. Pandolfo, M. The molecular basis of Friedreich ataxia. *Advances in experimental medicine and biology* **516**, 99-118 (2002).
17. Abrahao, A., *et al.* Milestones in Friedreich ataxia: more than a century and still learning. *Neurogenetics* **16**, 151-160 (2015).
18. Pandolfo, M. & Pastore, A. The pathogenesis of Friedreich ataxia and the structure and function of frataxin. *Journal of neurology* **256 Suppl 1**, 9-17 (2009).
19. Cossee, M., *et al.* Inactivation of the Friedreich ataxia mouse gene leads to early embryonic lethality without iron accumulation. *Human molecular genetics* **9**, 1219-1226 (2000).
20. Miranda, C.J., *et al.* Frataxin knockin mouse. *FEBS letters* **512**, 291-297 (2002).
21. Al-Mahdawi, S., *et al.* GAA repeat instability in Friedreich ataxia YAC transgenic mice. *Genomics* **84**, 301-310 (2004).

22. Al-Mahdawi, S.*, et al.* GAA repeat expansion mutation mouse models of Friedreich ataxia exhibit oxidative stress leading to progressive neuronal and cardiac pathology. *Genomics* **88**, 580-590 (2006).
23. Puccio, H.*, et al.* Mouse models for Friedreich ataxia exhibit cardiomyopathy, sensory nerve defect and Fe-S enzyme deficiency followed by intramitochondrial iron deposits. *Nature genetics* **27**, 181-186 (2001).
24. Simon, D.*, et al.* Friedreich ataxia mouse models with progressive cerebellar and sensory ataxia reveal autophagic neurodegeneration in dorsal root ganglia. *The Journal of neuroscience : the official journal of the Society for Neuroscience* **24**, 1987-1995 (2004).
25. Perdomini, M., Hick, A., Puccio, H. & Pook, M.A. Animal and cellular models of Friedreich ataxia. *Journal of neurochemistry* **126 Suppl 1**, 65-79 (2013).
26. Metz, G.*, et al.* Rating disease progression of Friedreich's ataxia by the International Cooperative Ataxia Rating Scale: analysis of a 603-patient database. *Brain : a journal of neurology* **136**, 259-268 (2013).
27. Patel, M.*, et al.* Progression of Friedreich ataxia: quantitative characterization over 5 years. *Annals of clinical and translational neurology* **3**, 684-694 (2016).
28. Seibler, J.*, et al.* Reversible gene knockdown in mice using a tight, inducible shRNA expression system. *Nucleic acids research* **35**, e54 (2007).
29. Crawley, J.N. *What's wrong with my mouse? : behavioral phenotyping of transgenic and knockout mice*, (Wiley-Interscience, Hoboken, N.J., 2007).
30. Dellon, E.S. & Dellon, A.L. Functional assessment of neurologic impairment: track analysis in diabetic and compression neuropathies. *Plastic and reconstructive surgery* **88**, 686-694 (1991).
31. Tsou, A.Y.*, et al.* Mortality in Friedreich ataxia. *Journal of the neurological sciences* **307**, 46-49 (2011).
32. Pousset, F.*, et al.* A 22-Year Follow-up Study of Long-term Cardiac Outcome and Predictors of Survival in Friedreich Ataxia. *JAMA neurology* **72**, 1334-1341 (2015).
33. Surawicz, B. & Knoebel, S.B. Long QT: good, bad or indifferent? *Journal of the American College of Cardiology* **4**, 398-413 (1984).
34. German, D.M., Kabir, M.M., Dewland, T.A., Henrikson, C.A. & Tereshchenko, L.G. Atrial Fibrillation Predictors: Importance of the Electrocardiogram. *Annals of noninvasive electrocardiology : the official journal of the International Society for Holter and Noninvasive Electrocardiology, Inc* **21**, 20-29 (2016).
35. Dutka, D.P., Donnelly, J.E., Nihoyannopoulos, P., Oakley, C.M. & Nunez, D.J. Marked variation in the cardiomyopathy associated with Friedreich's ataxia. *Heart* **81**, 141-147 (1999).
36. Isnard, R.*, et al.* Correlation between left ventricular hypertrophy and GAA trinucleotide repeat length in Friedreich's ataxia. *Circulation* **95**, 2247-2249 (1997).
37. Durr, A.*, et al.* Clinical and genetic abnormalities in patients with Friedreich's ataxia. *The New England journal of medicine* **335**, 1169-1175 (1996).
38. Conrad, C.H.*, et al.* Myocardial fibrosis and stiffness with hypertrophy and heart failure in the spontaneously hypertensive rat. *Circulation* **91**, 161-170 (1995).
39. Bradley, J.L.*, et al.* Clinical, biochemical and molecular genetic correlations in Friedreich's ataxia. *Human molecular genetics* **9**, 275-282 (2000).

40. Rotig, A., *et al.* Aconitase and mitochondrial iron-sulphur protein deficiency in Friedreich ataxia. *Nature genetics* **17**, 215-217 (1997).
41. Seyer, L.A., *et al.* Analysis of the visual system in Friedreich ataxia. *Journal of neurology* **260**, 2362-2369 (2013).
42. Fortuna, F., *et al.* Visual system involvement in patients with Friedreich's ataxia. *Brain : a journal of neurology* **132**, 116-123 (2009).
43. Saxena, S., Srivastav, K., Cheung, C.M., Ng, J.Y. & Lai, T.Y. Photoreceptor inner segment ellipsoid band integrity on spectral domain optical coherence tomography. *Clinical ophthalmology* **8**, 2507-2522 (2014).
44. Coppola, G., *et al.* A gene expression phenotype in lymphocytes from Friedreich ataxia patients. *Annals of neurology* **70**, 790-804 (2011).
45. Cartier, L., Hartley, O., Dubois-Dauphin, M. & Krause, K.H. Chemokine receptors in the central nervous system: role in brain inflammation and neurodegenerative diseases. *Brain research. Brain research reviews* **48**, 16-42 (2005).
46. Leszek, J., *et al.* Inflammatory Mechanisms and Oxidative Stress as Key Factors Responsible for Progression of Neurodegeneration: Role of Brain Innate Immune System. *CNS & neurological disorders drug targets* **15**, 329-336 (2016).
47. Fung, T.C., Olson, C.A. & Hsiao, E.Y. Interactions between the microbiota, immune and nervous systems in health and disease. *Nature neuroscience* (2017).
48. Andreasson, K.I., *et al.* Targeting innate immunity for neurodegenerative disorders of the central nervous system. *Journal of neurochemistry* **138**, 653-693 (2016).
49. Zhang, B. & Horvath, S. A general framework for weighted gene co-expression network analysis. *Statistical applications in genetics and molecular biology* **4**, Article17 (2005).
50. Langfelder, P. & Horvath, S. WGCNA: an R package for weighted correlation network analysis. *BMC bioinformatics* **9**, 559 (2008).
51. Geschwind, D.H. & Konopka, G. Neuroscience in the era of functional genomics and systems biology. *Nature* **461**, 908-915 (2009).
52. Zhang, B., *et al.* Integrated systems approach identifies genetic nodes and networks in late-onset Alzheimer's disease. *Cell* **153**, 707-720 (2013).
53. Parikshak, N.N., *et al.* Genome-wide changes in lncRNA, splicing, and regional gene expression patterns in autism. *Nature* (2016).
54. Haugen, A.C., *et al.* Altered gene expression and DNA damage in peripheral blood cells from Friedreich's ataxia patients: cellular model of pathology. *PLoS genetics* **6**, e1000812 (2010).
55. Aiyaz, M., Lupton, M.K., Proitsi, P., Powell, J.F. & Lovestone, S. Complement activation as a biomarker for Alzheimer's disease. *Immunobiology* **217**, 204-215 (2012).
56. Risgaard, B., *et al.* High prevalence of genetic variants previously associated with Brugada syndrome in new exome data. *Clinical genetics* **84**, 489-495 (2013).
57. Bienengraeber, M., *et al.* ABCC9 mutations identified in human dilated cardiomyopathy disrupt catalytic KATP channel gating. *Nature genetics* **36**, 382-387 (2004).
58. Singh, V.P., *et al.* Abnormal calcium cycling and cardiac arrhythmias associated with the human Ser96Ala genetic variant of histidine-rich calcium-binding protein. *Journal of the American Heart Association* **2**, e000460 (2013).

59. Gonzalez, A., *et al.* Cardiomyocyte apoptosis in hypertensive cardiomyopathy. *Cardiovascular research* **59**, 549-562 (2003).
60. Huang, M.L., *et al.* Elucidation of the mechanism of mitochondrial iron loading in Friedreich's ataxia by analysis of a mouse mutant. *Proceedings of the National Academy of Sciences of the United States of America* **106**, 16381-16386 (2009).
61. Bolinches-Amoros, A., Molla, B., Pla-Martin, D., Palau, F. & Gonzalez-Cabo, P. Mitochondrial dysfunction induced by frataxin deficiency is associated with cellular senescence and abnormal calcium metabolism. *Frontiers in cellular neuroscience* **8**, 124 (2014).
62. Muzio, M., *et al.* FLICE, a novel FADD-homologous ICE/CED-3-like protease, is recruited to the CD95 (Fas/APO-1) death--inducing signaling complex. *Cell* **85**, 817-827 (1996).
63. Kyrylkova, K., Kyryachenko, S., Leid, M. & Kioussi, C. Detection of apoptosis by TUNEL assay. *Methods in molecular biology* **887**, 41-47 (2012).
64. Trugenberger, C.A., Walti, C., Peregrim, D., Sharp, M.E. & Bureeva, S. Discovery of novel biomarkers and phenotypes by semantic technologies. *BMC bioinformatics* **14**, 51 (2013).
65. Vermeer, S., *et al.* Targeted next-generation sequencing of a 12.5 Mb homozygous region reveals ANO10 mutations in patients with autosomal-recessive cerebellar ataxia. *American journal of human genetics* **87**, 813-819 (2010).
66. Miskovic, N.D., *et al.* Seemingly dominant inheritance of a recessive ANO10 mutation in romani families with cerebellar ataxia. *Movement disorders : official journal of the Movement Disorder Society* (2016).
67. Mollet, J., *et al.* CABC1 gene mutations cause ubiquinone deficiency with cerebellar ataxia and seizures. *American journal of human genetics* **82**, 623-630 (2008).
68. Gerards, M., *et al.* Nonsense mutations in CABC1/ADCK3 cause progressive cerebellar ataxia and atrophy. *Mitochondrion* **10**, 510-515 (2010).
69. Schicks, J., Synofzik, M., Schulte, C. & Schols, L. POLG, but not PEO1, is a frequent cause of cerebellar ataxia in Central Europe. *Movement disorders : official journal of the Movement Disorder Society* **25**, 2678-2682 (2010).
70. Synofzik, M., Srulijes, K., Godau, J., Berg, D. & Schols, L. Characterizing POLG ataxia: clinics, electrophysiology and imaging. *Cerebellum* **11**, 1002-1011 (2012).
71. Pennacchio, L.A., *et al.* Progressive ataxia, myoclonic epilepsy and cerebellar apoptosis in cystatin B-deficient mice. *Nature genetics* **20**, 251-258 (1998).
72. Singh, S. & Ganesh, S. Lafora progressive myoclonus epilepsy: a meta-analysis of reported mutations in the first decade following the discovery of the EPM2A and NHLRC1 genes. *Human mutation* **30**, 715-723 (2009).
73. Matthijs, G., *et al.* Mutations in PMM2, a phosphomannomutase gene on chromosome 16p13, in carbohydrate-deficient glycoprotein type I syndrome (Jaeken syndrome). *Nature genetics* **16**, 88-92 (1997).
74. Sygitowicz, G., Tomaniak, M., Filipiak, K.J., Koltowski, L. & Sitkiewicz, D. Galectin-3 in Patients with Acute Heart Failure: Preliminary Report on First Polish Experience. *Advances in clinical and experimental medicine : official organ Wroclaw Medical University* **25**, 617-623 (2016).

75. Salvador, A.M., *et al.* Intercellular Adhesion Molecule 1 Regulates Left Ventricular Leukocyte Infiltration, Cardiac Remodeling, and Function in Pressure Overload-Induced Heart Failure. *Journal of the American Heart Association* **5**, e003126 (2016).
76. Polyakova, V., *et al.* Fibrosis in endstage human heart failure: severe changes in collagen metabolism and MMP/TIMP profiles. *International journal of cardiology* **151**, 18-33 (2011).
77. Del-Castillo-Rueda, A., *et al.* Mutations in the HFE, TFR2, and SLC40A1 genes in patients with hemochromatosis. *Gene* **508**, 15-20 (2012).
78. Song, W., *et al.* Unregulated brain iron deposition in transgenic mice over-expressing HMOX1 in the astrocytic compartment. *Journal of neurochemistry* **123**, 325-336 (2012).
79. Cui, R., *et al.* Serum iron metabolism and erythropoiesis in patients with myelodysplastic syndrome not receiving RBC transfusions. *Leukemia research* **38**, 545-550 (2014).
80. Pavel, M. & Rubinsztein, D.C. Mammalian autophagy and the plasma membrane. *The FEBS journal* (2016).
81. Bento, C.F., *et al.* Mammalian Autophagy: How Does It Work? *Annual review of biochemistry* **85**, 685-713 (2016).
82. Gustafsson, A.B. & Gottlieb, R.A. Autophagy in ischemic heart disease. *Circulation research* **104**, 150-158 (2009).
83. Perdomini, M., *et al.* Prevention and reversal of severe mitochondrial cardiomyopathy by gene therapy in a mouse model of Friedreich's ataxia. *Nature medicine* **20**, 542-547 (2014).
84. Gottesfeld, J.M., Rusche, J.R. & Pandolfo, M. Increasing frataxin gene expression with histone deacetylase inhibitors as a therapeutic approach for Friedreich's ataxia. *Journal of neurochemistry* **126 Suppl 1**, 147-154 (2013).
85. Delatycki, M.B., *et al.* Direct evidence that mitochondrial iron accumulation occurs in Friedreich ataxia. *Annals of neurology* **45**, 673-675 (1999).
86. Michael, S., *et al.* Iron and iron-responsive proteins in the cardiomyopathy of Friedreich's ataxia. *Cerebellum* **5**, 257-267 (2006).
87. Lynch, D.R., Deutsch, E.C., Wilson, R.B. & Tennekoon, G. Unanswered questions in Friedreich ataxia. *Journal of child neurology* **27**, 1223-1229 (2012).
88. Fujita, T. & Ishikawa, Y. Apoptosis in heart failure. -The role of the beta-adrenergic receptor-mediated signaling pathway and p53-mediated signaling pathway in the apoptosis of cardiomyocytes. *Circulation journal : official journal of the Japanese Circulation Society* **75**, 1811-1818 (2011).
89. Bennett, M.R. Apoptosis in the cardiovascular system. *Heart* **87**, 480-487 (2002).
90. Ravichandran, K.S. Beginnings of a good apoptotic meal: the find-me and eat-me signaling pathways. *Immunity* **35**, 445-455 (2011).
91. Martinet, W., Knaapen, M.W., Kockx, M.M. & De Meyer, G.R. Autophagy in cardiovascular disease. *Trends in molecular medicine* **13**, 482-491 (2007).
92. Eisenberg-Lerner, A., Bialik, S., Simon, H.U. & Kimchi, A. Life and death partners: apoptosis, autophagy and the cross-talk between them. *Cell death and differentiation* **16**, 966-975 (2009).
93. Tan, G., *et al.* Frataxin expression rescues mitochondrial dysfunctions in FRDA cells. *Human molecular genetics* **10**, 2099-2107 (2001).
94. Koutnikova, H., *et al.* Studies of human, mouse and yeast homologues indicate a mitochondrial function for frataxin. *Nature genetics* **16**, 345-351 (1997).

95. Foury, F. & Cazzalini, O. Deletion of the yeast homologue of the human gene associated with Friedreich's ataxia elicits iron accumulation in mitochondria. *FEBS letters* **411**, 373-377 (1997).
96. Lodi, R.*, et al.* Deficit of in vivo mitochondrial ATP production in patients with Friedreich ataxia. *Proceedings of the National Academy of Sciences of the United States of America* **96**, 11492-11495 (1999).
97. Gonzalez-Cabo, P. & Palau, F. Mitochondrial pathophysiology in Friedreich's ataxia. *Journal of neurochemistry* **126 Suppl 1**, 53-64 (2013).
98. Chan, D.C. Fusion and fission: interlinked processes critical for mitochondrial health. *Annual review of genetics* **46**, 265-287 (2012).
99. Desagher, S. & Martinou, J.C. Mitochondria as the central control point of apoptosis. *Trends in cell biology* **10**, 369-377 (2000).
100. Goodman, J.M. The gregarious lipid droplet. *The Journal of biological chemistry* **283**, 28005-28009 (2008).
101. Tarnopolsky, M.A.*, et al.* Influence of endurance exercise training and sex on intramyocellular lipid and mitochondrial ultrastructure, substrate use, and mitochondrial enzyme activity. *American journal of physiology. Regulatory, integrative and comparative physiology* **292**, R1271-1278 (2007).
102. Vyas, P.M.*, et al.* A TAT-frataxin fusion protein increases lifespan and cardiac function in a conditional Friedreich's ataxia mouse model. *Human molecular genetics* **21**, 1230-1247 (2012).
103. Rufini, A.*, et al.* Highly specific ubiquitin-competing molecules effectively promote frataxin accumulation and partially rescue the aconitase defect in Friedreich ataxia cells. *Neurobiology of disease* **75**, 91-99 (2015).
104. Coppola, G.*, et al.* Gene expression profiling in frataxin deficient mice: microarray evidence for significant expression changes without detectable neurodegeneration. *Neurobiology of disease* **22**, 302-311 (2006).
105. Shen, Y.*, et al.* Frataxin Deficiency Promotes Excess Microglial DNA Damage and Inflammation that Is Rescued by PJ34. *PloS one* **11**, e0151026 (2016).
106. Lu, C.*, et al.* Frataxin deficiency induces Schwann cell inflammation and death. *Biochimica et biophysica acta* **1792**, 1052-1061 (2009).
107. Strawser, C.J., Schadt, K.A. & Lynch, D.R. Therapeutic approaches for the treatment of Friedreich's ataxia. *Expert review of neurotherapeutics* **14**, 949-957 (2014).
108. Sandi, C., Sandi, M., Anjomani Virmouni, S., Al-Mahdawi, S. & Pook, M.A. Epigenetic-based therapies for Friedreich ataxia. *Frontiers in genetics* **5**, 165 (2014).
109. Kearney, M., Orrell, R.W., Fahey, M., Brassington, R. & Pandolfo, M. Pharmacological treatments for Friedreich ataxia. *The Cochrane database of systematic reviews*, CD007791 (2016).

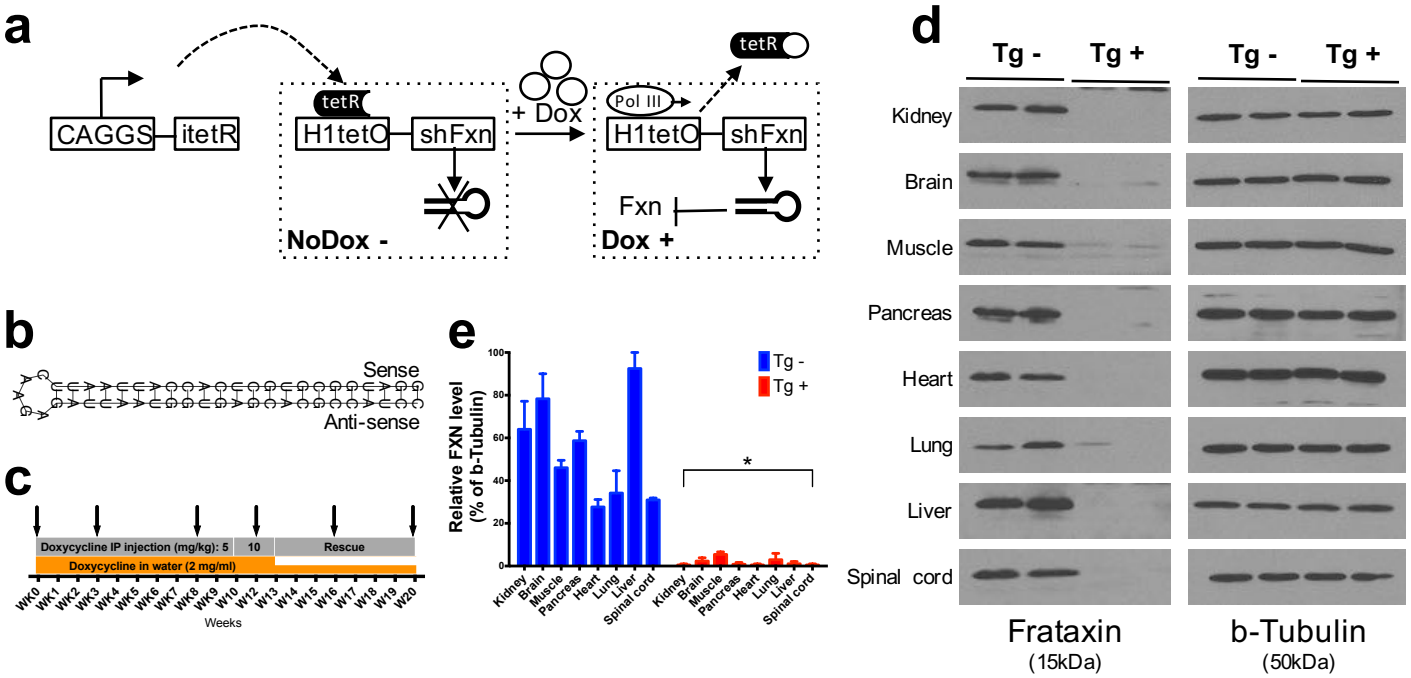
a
CAGGS
itetR
tetR
H1tetO
shFxn
NoDox -
+ Dox
Pol III
tetR
H1tetO
shFxn
Fxn
Dox +
b
Sense
Anti-sense
c
Doxycycline IP injection (mg/kg): 5
10
Rescue
Doxycycline in water (2 mg/ml)
Weeks
e
Relative FXN level (% of b-Tubulin)
Tg -
Tg +
Kidney
Brain
Muscle
Pancreas
Heart
Lung
Liver
Spinal cord
d
Tg -
Tg +
Kidney
Brain
Muscle
Pancreas
Heart
Lung
Liver
Spinal cord
Frataxin
(15kDa)
b-Tubulin
(50kDa)

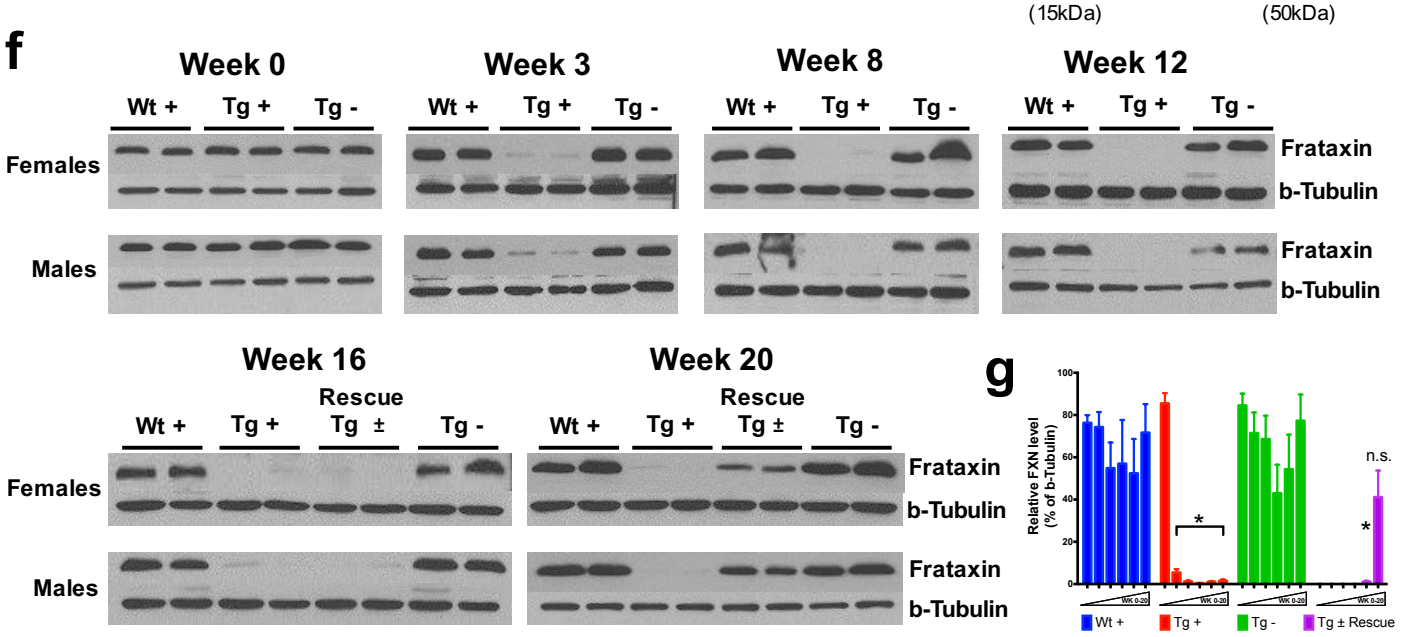
f
Week 0
Week 3
Week 8
Week 12
Wt +
Tg +
Tg -
Females
Males
Frataxin
b-Tubulin
Week 16
Week 20
Rescue
Tg ±
g
Relative FXN level (% of b-Tubulin)
n.s.
Wt +
Tg +
Tg -
Tg ± Rescue

Figure 1

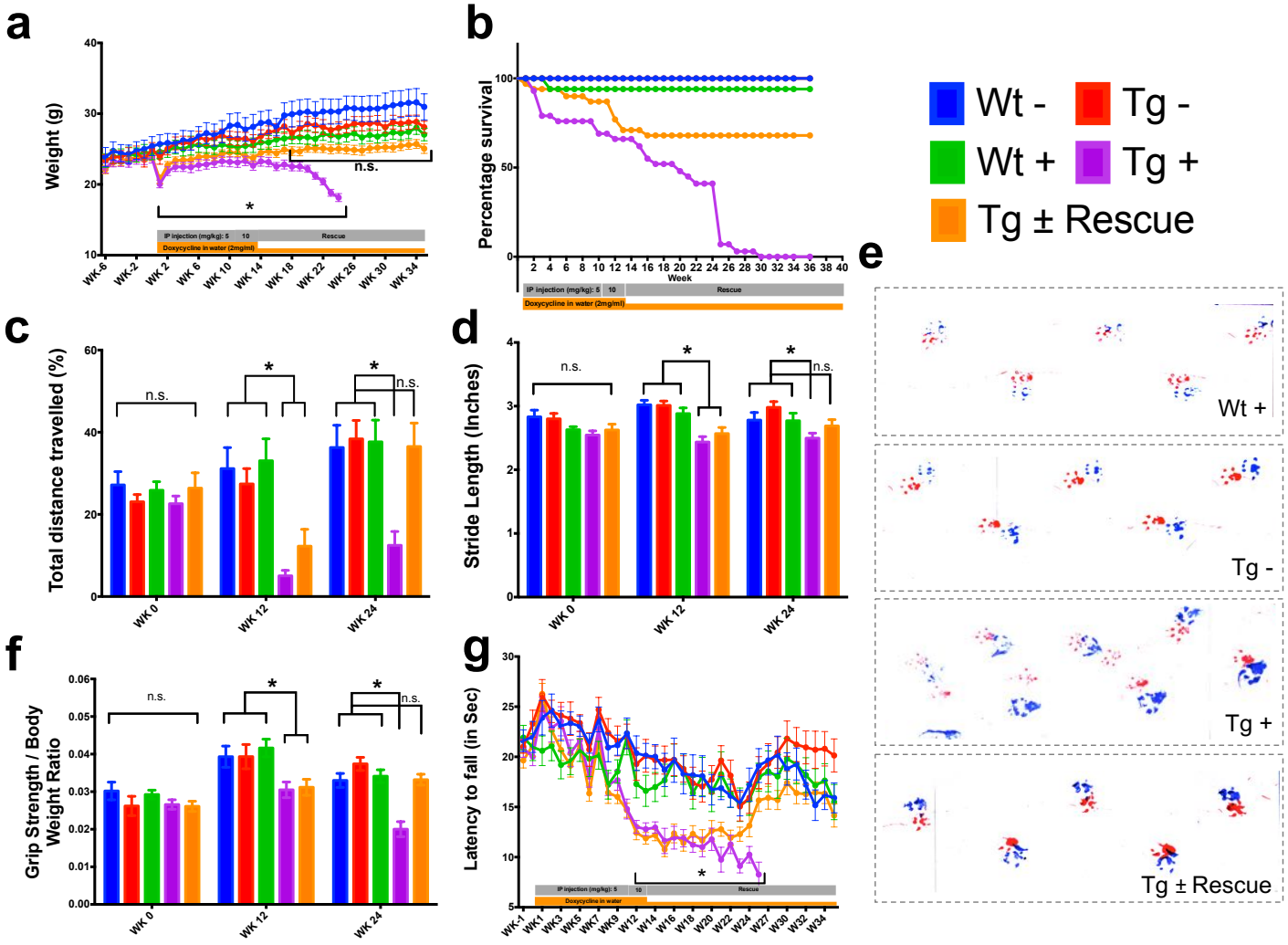
a
Weight (g)
n.s.
*
IP injection (mg/kg): 5
10
Rescue
Doxycycline in water (2mg/ml)
WK-6
WK-2
WK 2
WK 6
WK 10
WK 14
WK 18
WK 22
WK 26
WK 30
WK 34
b
Percentage survival
Week
IP injection (mg/kg): 5
10
Rescue
Doxycycline in water (2mg/ml)
Wt -
Tg -
Wt +
Tg +
Tg ± Rescue
e
Wt +
Tg -
Tg +
Tg ± Rescue
c
Total distance travelled (%)
n.s.
*
*
n.s.
WK 0
WK 12
WK 24
d
Stride Length (Inches)
n.s.
*
*
n.s.
WK 0
WK 12
WK 24
f
Grip Strength / Body Weight Ratio
n.s.
*
*
n.s.
WK 0
WK 12
WK 24
g
Latency to fall (in Sec)
*
IP injection (mg/kg): 5
10
Rescue
Doxycycline in water
WK-1
WK1
WK3
WK5
WK7
WK9
W12
W14
W16
W18
W20
W22
W24
W27
W30
W32
W34

Figure 2

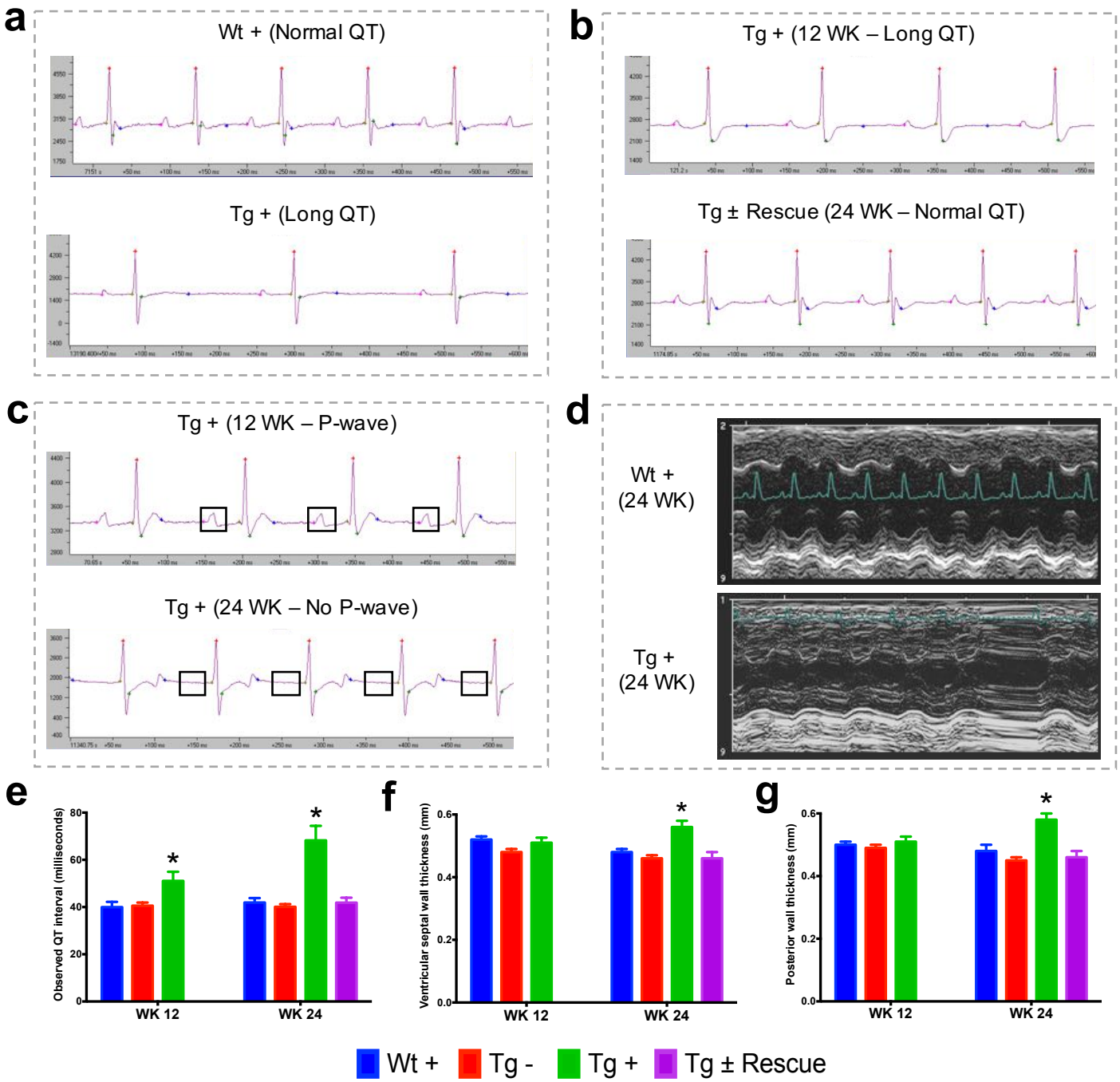
a
Wt + (Normal QT)
Tg + (Long QT)
b
Tg + (12 WK – Long QT)
Tg ± Rescue (24 WK – Normal QT)
c
Tg + (12 WK – P-wave)
Tg + (24 WK – No P-wave)
d
Wt +
(24 WK)
Tg +
(24 WK)
e
Observed QT interval (milliseconds)
WK 12
WK 24
f
Ventricular septal wall thickness (mm)
WK 12
WK 24
g
Posterior wall thickness (mm)
WK 12
WK 24
Wt +
Tg -
Tg +
Tg ± Rescue

Figure 3

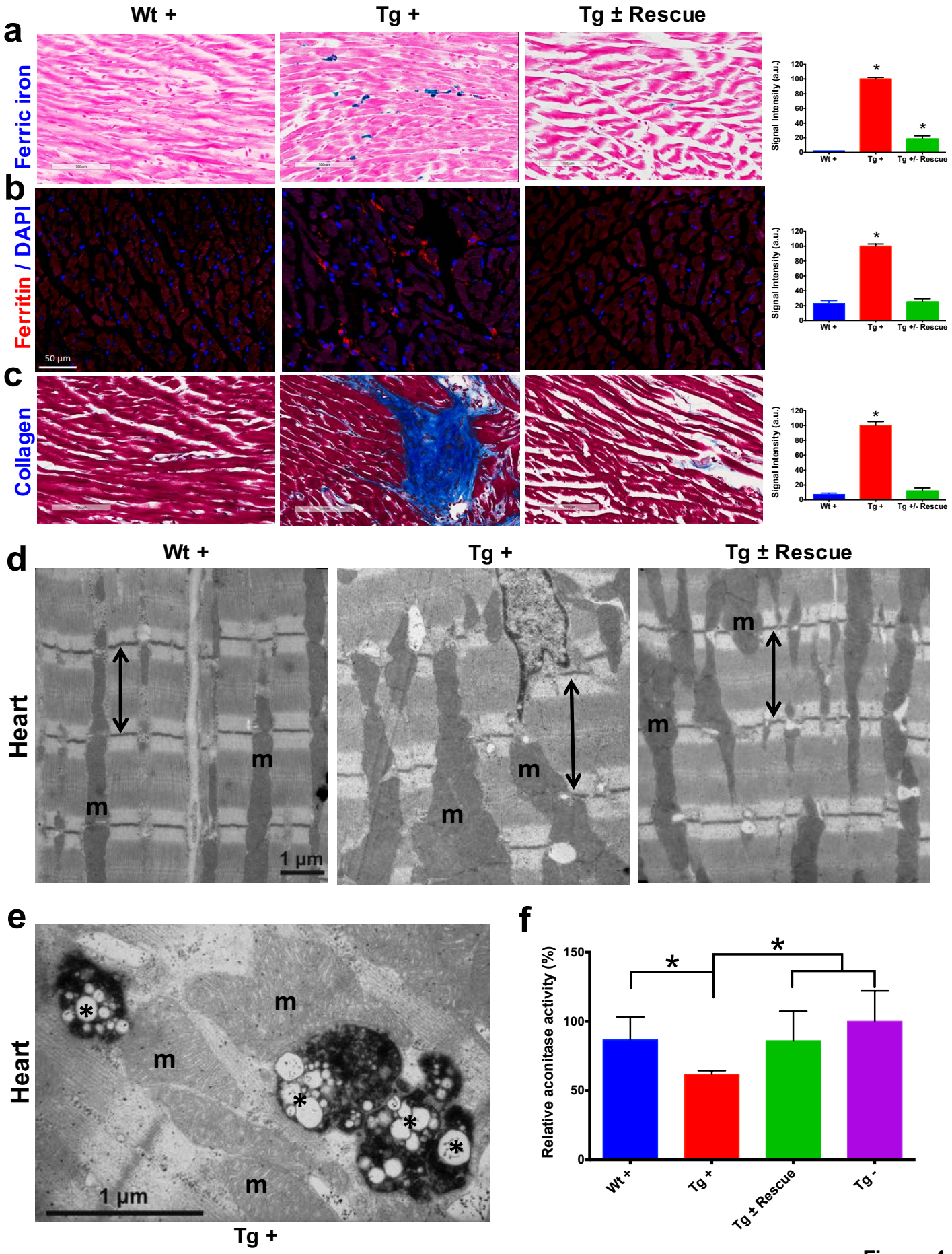
a
Wt +
Tg +
Tg ± Rescue
Ferric iron
Signal Intensity (a.u.)
Wt +
Tg +
Tg +/- Rescue
b
Ferritin / DAPI
50 µm
c
Collagen
d
Heart
m
1 µm
e
Heart
1 µm
Tg +
f
Relative aconitase activity (%)
Wt +
Tg +
Tg ± Rescue
Tg -

Figure 4

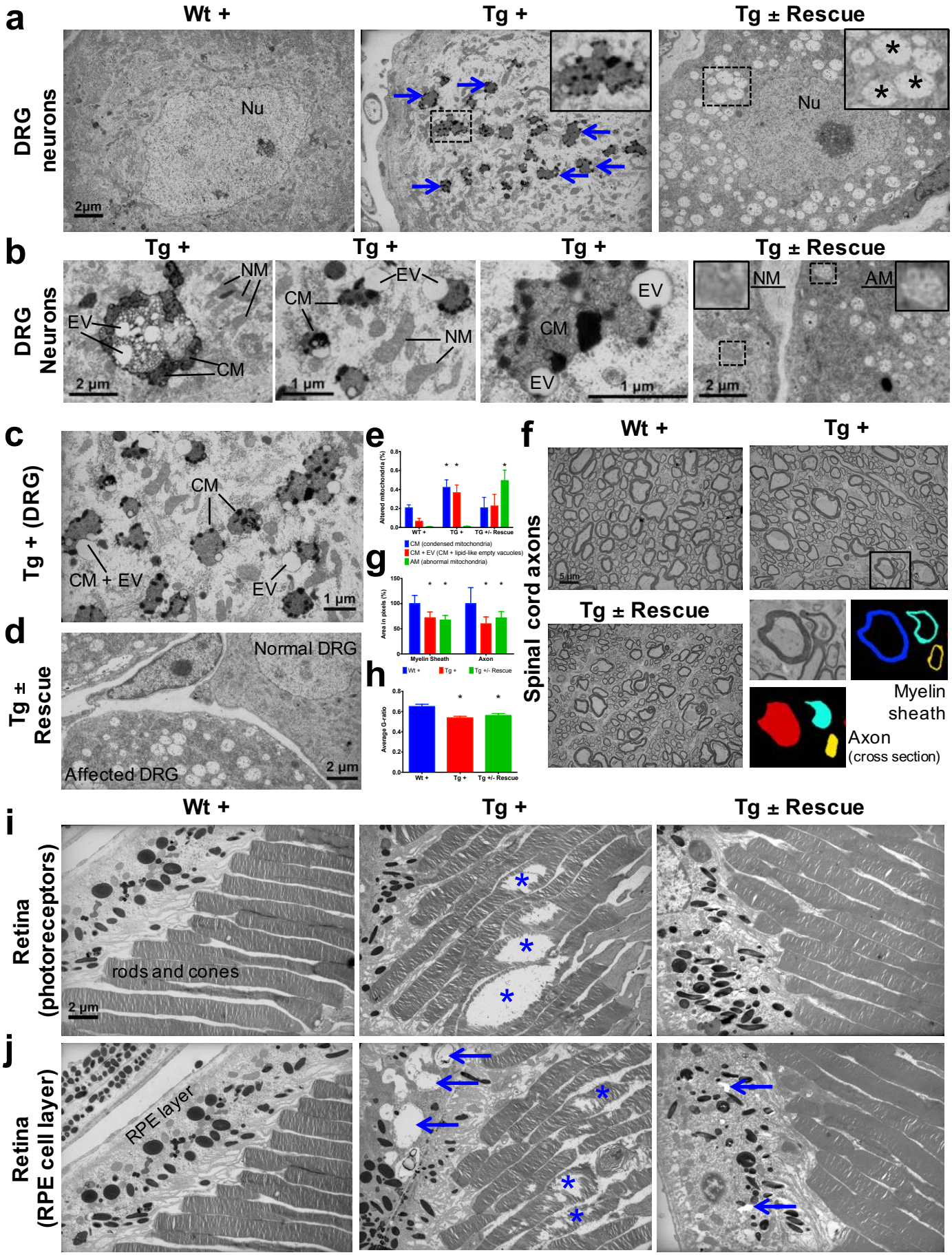
a
Wt +
Tg +
Tg ± Rescue
DRG neurons
Nu
2µm
b
Tg +
Tg +
Tg +
Tg ± Rescue
DRG Neurons
NM
EV
CM
2 µm
1 µm
AM
c
Tg + (DRG)
CM + EV
d
Tg ± Rescue
Normal DRG
Affected DRG
e
Altered mitochondria (%)
CM (condensed mitochondria)
CM + EV (CM + lipid-like empty vacuoles)
AM (abnormal mitochondria)
g
Area in pixels (%)
Myelin Sheath
Axon
h
Average G-ratio
f
Spinal cord axons
5 µm
Myelin sheath
Axon
(cross section)
i
Retina (photoreceptors)
rods and cones
j
Retina (RPE cell layer)
RPE layer

Figure 5

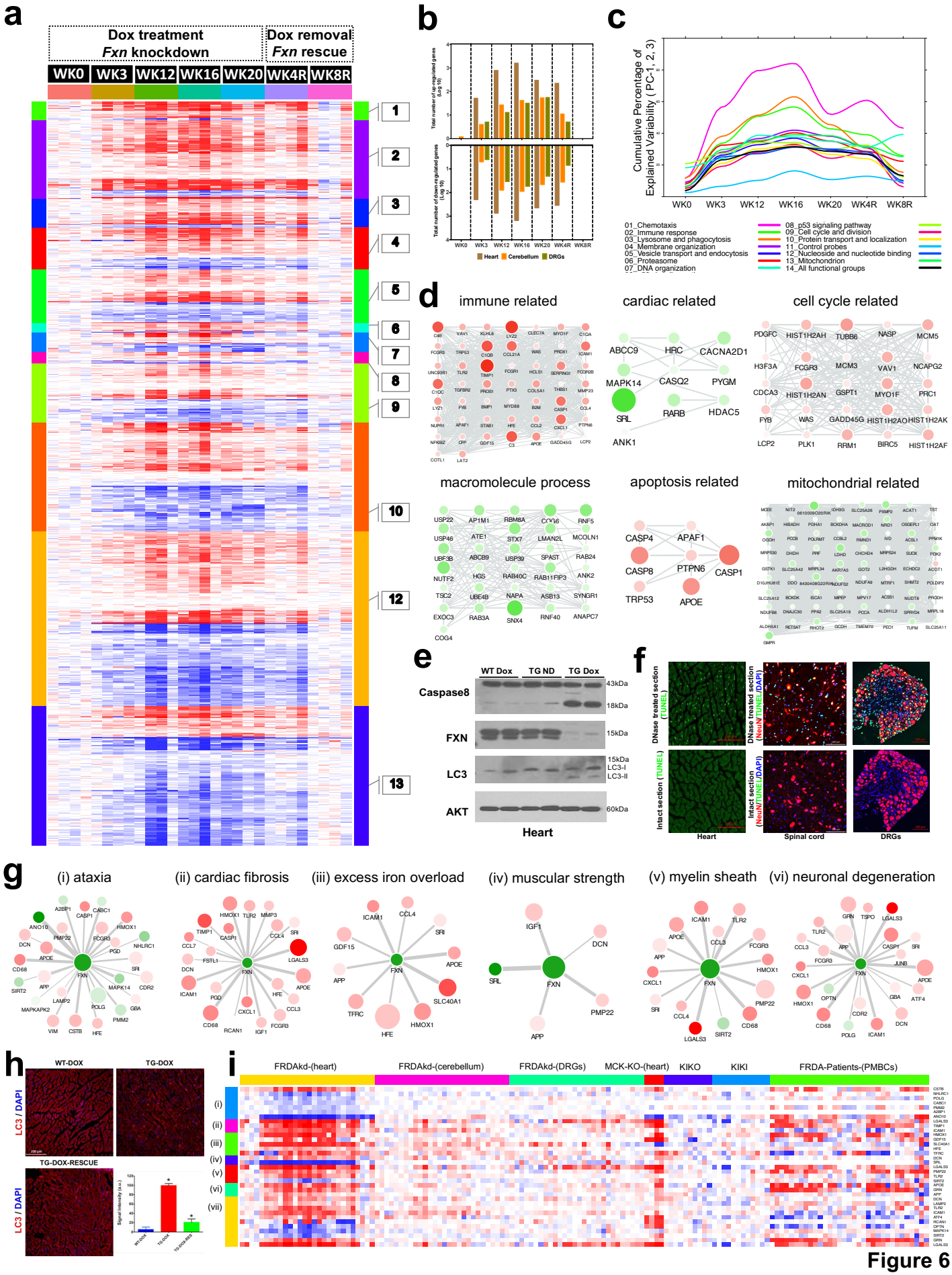
a
Dox treatment
Fxn knockdown
Dox removal
Fxn rescue
WK0
WK3
WK12
WK16
WK20
WK4R
WK8R
1
2
3
4
5
6
7
8
9
10
12
13
b
Total number of up-regulated genes (Log 10)
Total number of down-regulated genes (Log 10)
Heart
Cerebellum
DRGs
c
Cumulative Percentage of Explained Variability (PC-1, 2, 3)
01_Chemotaxis
02_Immune response
03_Lysosome and phagocytosis
04_Membrane organization
05_Vesicle transport and endocytosis
06_Proteasome
07_DNA organization
08_p53 signaling pathway
09_Cell cycle and division
10_Protein transport and localization
11_Control probes
12_Nucleoside and nucleotide binding
13_Mitochondrion
14_All functional groups
d
immune related
cardiac related
cell cycle related
macromolecule process
apoptosis related
mitochondrial related
e
WT Dox
TG ND
TG Dox
Caspase8
43kDa
18kDa
FXN
15kDa
LC3
15kDa
LC3-I
LC3-II
AKT
60kDa
Heart
f
DNase treated section (TUNEL)
DNase treated section (NeuN/TUNEL/DAPI)
Intact section (TUNEL)
Intact section (NeuN/TUNEL/DAPI)
Heart
Spinal cord
DRGs
g
(i) ataxia
(ii) cardiac fibrosis
(iii) excess iron overload
(iv) muscular strength
(v) myelin sheath
(vi) neuronal degeneration
h
WT-DOX
TG-DOX
TG-DOX-RESCUE
LC3 / DAPI
i
FRDAkd-(heart)
FRDAkd-(cerebellum)
FRDAkd-(DRGs)
MCK-KO-(heart)
KIKO
KIKI
FRDA-Patients-(PMBCs)
(i)
(ii)
(iii)
(iv)
(v)
(vi)
(vii)

Figure 6